Development of Laboratory and Field Drilling Tools to Measure Bit Operating

Conditions and Drill String Motions

by

© Qian Gao

A Thesis submitted to the

School of Graduate Studies

in partial fulfillment of the requirements for the degree of

Master of Engineering

Faculty of Engineering and Applied Science

Memorial University of Newfoundland

May, 2015

St.John's   Newfoundland and Labrador

ABSTRACT

The Advanced Drilling Laboratory (ADL) has been developing a Vibration Assisted Rotary Drilling (VARD) System for several years, which is used for seeking the advantages brought by combining drilling bit vibration and rotation together in drilling operation. In order to achieve the laboratory and field data acquisition and processing, several integrated data acquisition systems are necessary. These systems are based on the most suitable sensors, acquisition parameters, and software to monitor different bit operating conditions and drill string motions in different experiments.

The laboratory and field measurement systems include i) the control system of a Small Drilling Simulator (SDS), ii) a Mobile Data Acquisition system for field experiments, and iii) a Down Hole Measurement Tool, or Sensor Sub for drilling field trials.

The system for the SDS is based on the LabVIEW programming language and includes the data acquisition, processing and system control ability. In this system, the LabVIEW user interface allows the operator to perform data acquisition, processing and logging.

The Mobile data acquisition (DAQ) system is an extension of the SDS system based on the Signal Express Program and includes data acquisition and processing. It was designed to be able to be carried and operated in tough environments and has numerous data acquisition configurations for a range of different experimental requirements.

The Down Hole Measurement Tool (Sensor Sub) is based on the use of accelerometers and magnetometers, along with onboard data acquisition and battery power systems; it is designed to operate in the down-hole environment with high

temperature, high pressure and severe vibration to supply raw data for each drilling experiment. The field trial results show that the Sensor Sub can provide compatible and accurate data to identify drill string motions (including rotary speed and bit orientation), and bit vibrations (including axial lateral torsional and bit whirl).

ACKNOWLEDGEMENTS

Table of Contents

List of Figures

List of Tables

List of Symbols, Nomenclature and Abbreviations

ADL   Advanced Drilling Laboratory

AIM   At-bit Inclination Measurement

API   American Petroleum Institute

DAQ   Data Acquisition System

DEM   Discrete Element Method

DVMCS   Drilling Vibration Monitoring & Control System

IDEAL   Integrated Drilling Evaluation and Logging

LPT   Linear Potential Transducer

MWD   Measurement While Drilling

NG   Natural Gas

PDC   Polycrystalline Diamond Compact

PDMM   Positive Displacement Mud Motor

RC   Roller Cone

ROP   Rate of Penetration

RPM   Revolutions per Minute

S.I.   International System of Units (metric system)

SDS   Small Scale Drilling Simulator prototype I

SWD   Seismic While Drilling

VARD   Vibration Assisted Rotary Drilling

VFD   Variable Frequency Drive

WOB   Weight on Bit

BHA   Bottom Hole Assembly

BHP   Bottom Hole Pressure

1. Introduction

1.1. Introduction

For most oil and gas exploitation activities, drilling is the most costly one. With more and more reservoirs being discovered offshore, in deep water and Arctic harsh environments, the drilling cost is increasing as well. For instance, the expense of the jack-up rigs offshore are around $1 million per day and the daily cost of floating rigs are ranging from $2.6 million to $5 million depending on their capability[1].

For the purpose of controlling the drilling cost, a very common way is to increase the drilling efficiency, which can be achieved by increasing the rate of penetration (ROP). The Advanced Drilling Laboratory (ADL) of Memorial University of Newfoundland is conducting a Vibration Assisted Rotary Drilling (VARD) testing to find out how to reach a higher ROP by adding vibration to the drill bit. Meanwhile, the laboratory tests require different data acquisition systems, and the development of these systems will be discussed in this thesis.

1.2. Research scope and objective

The Advanced Drilling Laboratory has been developing a Vibration Assisted Rotary Drilling (VARD) system during a comprehensive 7-year R&D program. This program is seeking the advantages brought by combining drilling bit vibration and rotation together in drilling operations. In order to achieve the laboratory and field data acquisition and processing, several integrated data acquisition systems are necessary. They are needed for different experiment environments and based on the most suitable program language.

Their function may include data acquisition, data processing and system control, depending on different experiment requirements.

One system is the data acquisition and control system on the Small Drilling Simulator (SDS). In 2011, an upgrade to the previous sensing and data acquisition system on the SDS was initiated. During the upgrading process, more sensors and the LabVIEW software were added into the system. Moreover, in order to increase the intelligence and safety of the system, a remote control system and an emergency stop system were added as well. The upgraded system is an integrated DAQ system which can be operated for different experimental purposes with a control function. The whole system is based on LabVIEW software and has three emergency stop buttons to enhance the operation safety.

Another system is a mobile DAQ system designed for field trial in 2012. The lab DAQ system is based on a PC and all the function and the connection are specially designed for the SDS, which is all hard-wired. There is a demand to develop a DAQ system which is easy to install and uninstall, has the capacity to do data recording for different sensors and also is able to function in various field operation environments. Due to these reasons, a mobile DAQ system needs to be built. The whole system is designed in two parts: one is the mobile power supply and the other is the mobile DAQ system. These two parts are separately installed in two Pelican watertight protective cases, which are able to be easily carried in any kinds of field environments.

The last DAQ system is a down-hole measurement tool (Sensor Sub) for the drilling field trials conducted in 2014, which is going to test the VARD technology and provide data to evaluate models of bit wear and drill string motions. The commercial drilling

tool (black box) for down-hole data recording can only give out the data after the internal process, but it cannot be used in experiments for lacking of raw data, so a down-hole measurement tool (Sensor Sub) is needed to record the down-hole vibration in raw data format. The Sensor Sub is designed based on the Arduino platform and uses three tri-axial accelerometers and one magnetometer to measure the down-hole vibration and rotation. In addition, all the raw data are saved on one micro-SD card and the whole system is powered by three parallel packs of AA batteries.

1.3. Research Background

In the past seven years, the VARD project has conducted several different experiments and achieved several milestones.

Li et al. [2] concluded a few observations after a series of experiments:

- ROP can be significantly increased by adding vibration to the bit.

- The founder point of the ROP-WOB (weight on bit) relation decreases while the vibration amplitude increases, which indicates that the same ROP can be achieved by a smaller WOB by adding axial vibration to the bit.

- ROP is proportional to vibration amplitude.

After Li's experiment, Babatunde et al. [3] used three different amplitude and frequency values in their experiments and they observed the same results: higher amplitude leads to higher ROP. Moreover, the experiments were conducted with a polycrystalline diamond compact (PDC) bit two cutting blades and two nozzles. The observations are:

- ROP can be improved by adding vibration to the PDC bit

- Lower WOB has an higher optimum vibration frequency (65Hz) and higher WOB's optimum frequency is lower (55Hz)

- Frequency peak was achieved at 9Hz

- The 9Hz was assumed to be due to the mechanical interaction between the rock and the PDC bit at a constant motor speed. Moreover, the optimum frequencies around multiples of 9Hz were assumed to be happening at some resonance of excited and natural vibrations.

In 2012, Pronin [4] did his experiment on a cavitation tool, using cavitation as a means of vibration source, and it was considered as an active VARD tool, which could generate vibration from itself, and he found:

- The vibration generated by the prototype only depends on the inlet pressure.

- The prototype produces significant outlet pressure pulses, which exceed the inlet pressure.

In 2013, Babapour and Butt [5] conducted a series of experiments utilizing the Pulses Cavitation Tool and they found that the cavitating pressure pulses generated by the tool can enhance the ROP if the drilling system is not rigid. In addition, Gharibiyamchi's simulation results [6] on Discrete Element Method (DEM) modelling match these results.

1.4. Significance of Research

In the past seven years, Advanced Drilling Laboratory members have done a lot of testing in our laboratory environment. Along with the test, laboratory development also made great progress. Among all the experiments mentioned in previous section, three

out of seven experiments utilized the data acquisition system and control system on SDS, and other two experiments utilized the Mobile DAQ system. Both of these two systems will be described in this thesis.

Up to now, all the experiments that have been done in the Advanced Drilling Laboratory have shown positive results; not only were the experiments conducted in the laboratory environment, but also in the field environment. Up to September 2014, we have drilled several hundred-metre deep wells and recorded the vibrations at the bit, and compared the results with and without the VARD tool, and we found that the VARD tool could significantly enhance the ROP.

However, the commercial drilling tool for data recording down-hole only gives out the processed data. If the daily renting rate is too high, it is not good for our experiment usage, so a down-hole measurement tool (Sensor Sub) was developed to record the down-hole vibration in the raw data format. This measurement tool was equipped with three tri-axial accelerometers, one tri-axial magnetometer, and onboard storage. The measurement tool deploys an aluminum alloy to avoid interference from the Earth's magnetic field. Furthermore, the arrangement of the sensors can make sure that the measurement tool can obtain the axial, torsional, and lateral vibration and azimuth of the tool faces. Additionally, without rotation, if we slide the tool down hole, we can utilize the magnetometer data cross-correlated with accelerometer data to get the inclination of the well.

2.   Literature Review

2.1. Development of the Drilling Operation Monitoring System in Drilling Industry

In the early stages of the drilling industry, before automation was applied, drillers depended on their own experience only to control the drilling, like determining the torque of the top drive, the flow rate of drilling fluid and the time of tripping out to change the bit, and so on. Humans are not as efficient as computers in calculation and reaction. If any incident happens, like kick, drilling fluid lost, or stick-slip, human always react slower than the computer-controlled systems. These incidents are dangerous and may lead to big accidents. Since the 1960s, intelligent control systems have been on the stage of the drilling industry.

Rowsell and Waller [7] developed an Intelligent Control Drilling System on a laboratory scale. This system is able to minimize the operation cost, self-optimize, predict the wear, carry out close loop control and sense the rock change.

In 2006, Qin Hu and Qingyou Liu [8] conducted research on the new technology by using an integrated drilling system to enhance the drilling efficiency in order to further control the operation cost.

In 2012, Arnaout et al [9] utilized sensors to measure the hock load, block position, flow rate, pump pressure, borehole and bit depth, revolutions per minute (RPM), torque, rate of penetration and weight on bit. The data collected from the mud-logging system were used to detect different drilling operations, and the surface sensor measurements can provide the information of drilling operations. Based on the information measured

through a number of drilling operations with different parameters, they summarized patterns to recognize and classify drilling operations upon receiving the data.

2.2. Downhole vibration monitoring systems

Downhole vibration monitoring systems are usually installed in the drill string or at the bit to measure the vibrations while drilling. The monitoring systems work without interrupting the drilling activity, so it is one type of Measurement While Drilling (MWD) System.

This section will describe several down-hole measurement tools developed in the past two decades, and they can somewhat reflect what improvements have been made in the petroleum industry. Although these tools are designed for different applications, they all face a severe down-hole operation environment. Therefore, the design of the tools has to meet the survival requirement, which is also important in our tool design. Moreover, the different design or arrangement of these tools and the utilization of the sensors provide us with valuable experience for our future work.

2.2.1. IDEAL System

In 1993, a new drilling technology was introduced in order to improve the drilling efficiency especially in the extended reach and horizontal applications. It was called the Integrated Drilling Evaluation and Logging technology (IDEAL system)[10]. This technology integrated "at-the-bit" measurement technology to provide Bit Resistivity, Azimuthal Resistivity, Focused Gamma Ray, Inclination and Motor RPM. These data

were transmitted to surface in real time to help optimize the wellbore trajectories, avoid problems with oil water contact, and adjust the direction of drilling.

Measurements at the Bit
- Bit Resistivity
- Azimuthal Resistivity
- Focused Gamma Ray
- Inclination
- Motor RPM
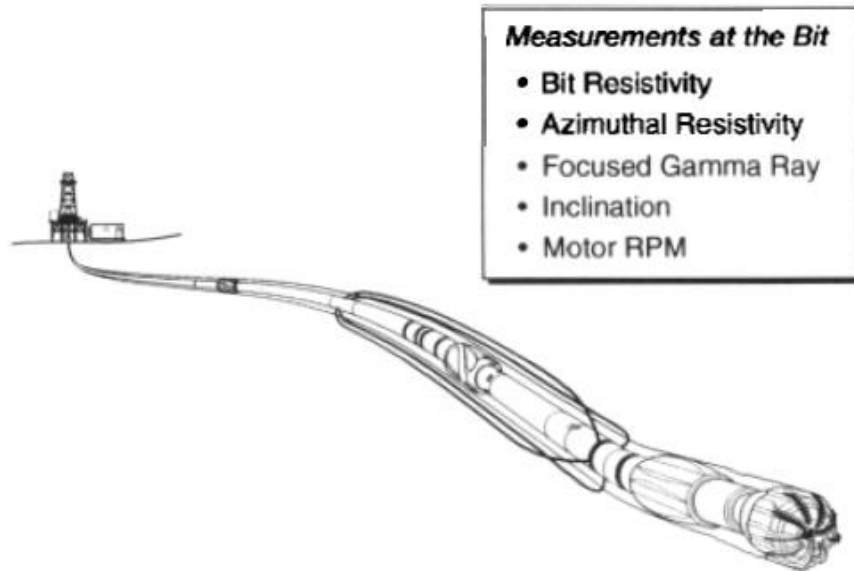
Figure 1 Instrumented Steerable Motor (IDEAL System) [10]

2.2.2. AIM System

In 2000, another behind-the-bit measurement system was developed. This tool is called At-bit Inclination Measurement (AIM) [11] tool, which was made by Schlumberger. This system includes a single axis inclinometer 0.3m behind the bit, and the sensor is mounted in the center of the rotating stabilizer. It was designed to improve the directional control and the drilling efficiency of the steerable positive displacement mud motors (PDMM). Figure 2 shows the arrangement of the sensor package in the AIM tool.

8
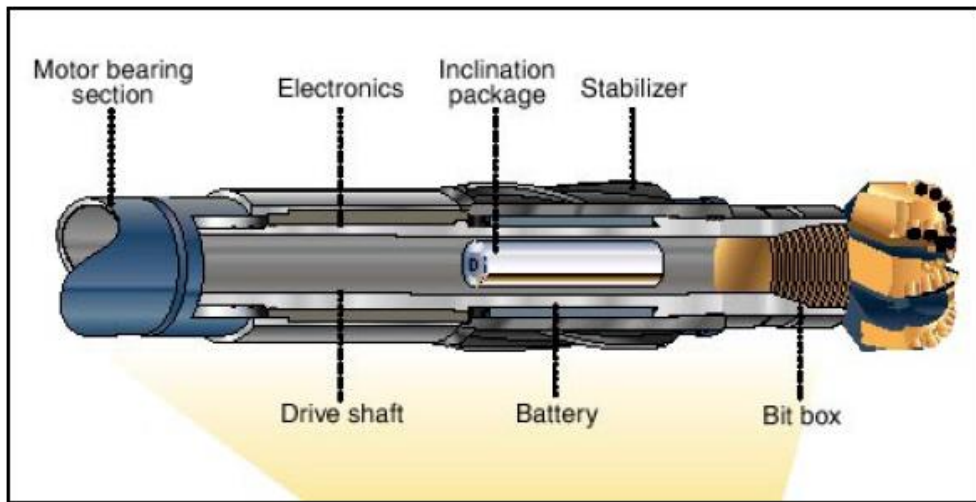
Figure 2 Schematic of AIM Tool [11]

2.2.3. Drill-string Dynamic Sensor

These systems are designed to provide the demanded data from the down-hole environment. Moreover, for down-hole drilling dynamic monitoring purposes, some other systems were developed too. In 1993, Zannoni et al. developed a new downhole MWD drill string dynamics sensor [12] to detect the harmful Bottom Hole Assembly (BHA) dynamic conditions such as whirling, lateral BHA shocks, stick-slip, and bit bounce.

This system mounted three accelerometers on an existing MWD tool, as shown in Figure 3, and was put 0.55m behind the Gamma Ray sub. The three accelerometers are placed mutually orthogonal and the orientations are shown in Figure 4[12].

In this design, they used the X-axis to measure both lateral and radial accelerations, the Y-axis to measure both lateral and tangential acceleration, and the Z-axis to measure

axial acceleration. Figure 5 illustrates the vector components of the three accelerometers of the Drill-string Dynamics Sensor.
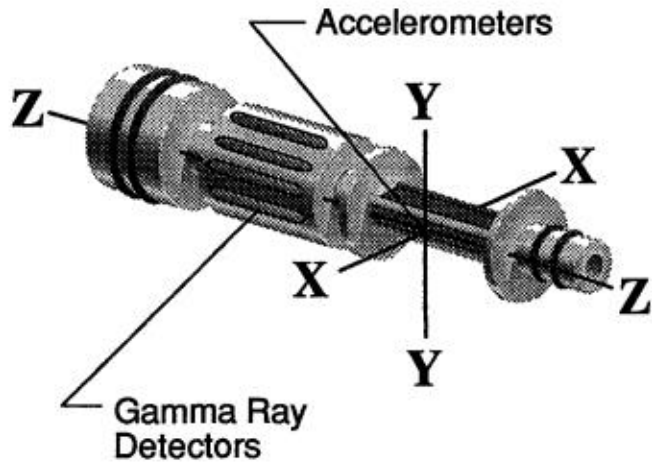
Figure 3 Drill-string Dynamics Sensor [12]
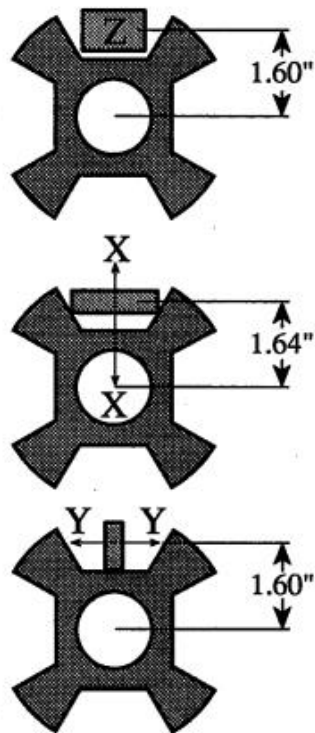
Figure 4 Accelerometer Orientation [12]
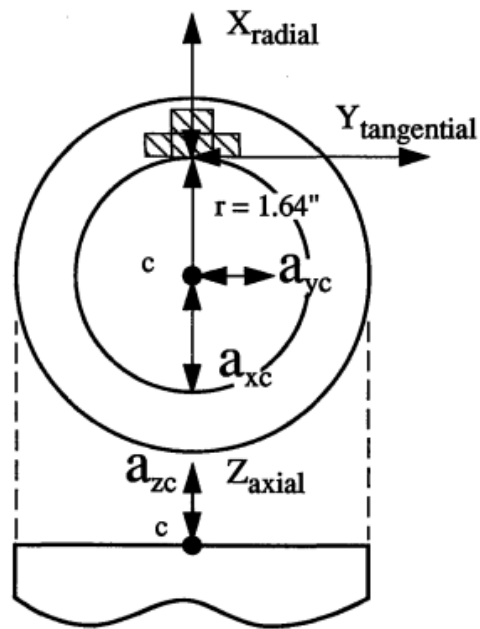
Figure 5 Accelerometer Vectors [12]

2.2.4. Diagnostic-While-Drilling (DWD) System

In 2003, Finger et al [13] and Mansure et al [14] invented the Diagnostic-While-Drilling System, which could provide high-speed, real-time downhole data while drilling.

This system contains a measurement sub, which comprises the following measurements [13]:

- Tri-axial acceleration

- High frequency axial acceleration

- Angular acceleration

- Magnetometer (rotary speed)

- Weight on bit, torque on bit, bending moment

- Drilling pipe and annulus pressure

- Drill pipe and annulus temperature

The measurement sub is a 17.8cm diameter by 2.16m long tubular tool, with a central sensor package (Figure 6). Strain gauges on the tool were designed for torque measurement, bending moment and weight on the bit measurement. Accelerometers and other electronics are mounted in the central package to measure the vibrations down-hole.

This system also utilized the magnetometer data to determine the rotary speed, which is risky, because the magnetometer reading might experience interference from the formation magnetic field or the iron element in the tool itself.
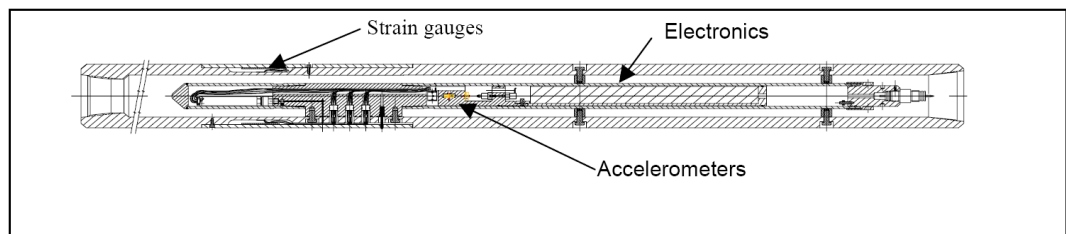
Figure 6 Layout of DWD measurement Sub [13]

2.2.5. Drilling Vibration Monitoring & Control System

In 2004, Cobern and Wassell published a paper on the design, modeling and laboratory testing of the Drilling Vibration Monitoring & Control System (DVMCS)[15], which is composed of a sensor package and a damping control system. The sensor package contains four single-axis accelerometers and one magnetometer. Three of the accelerometers are placed on the same section and are 120° apart from each other, and

the fourth accelerometer is set to measure the axial acceleration. The magnetometer is used as a backup to measure the rotary speed. The sensor arrangement is shown in Figure 7.

The algorithm used to calculate the lateral and tangential vibrations are based on the rotary speed, which is calculated from the centripetal acceleration. However, the accelerometers will also pick up the lateral vibration at the same time, so the equation $A_c(t) = \frac{A_1(t)+A_2(t)+A_3(t)}{3}$ used to calculate centripetal acceleration might not be reliable. In this case, the rotary speed calculated from centripetal acceleration will not be reliable as well.
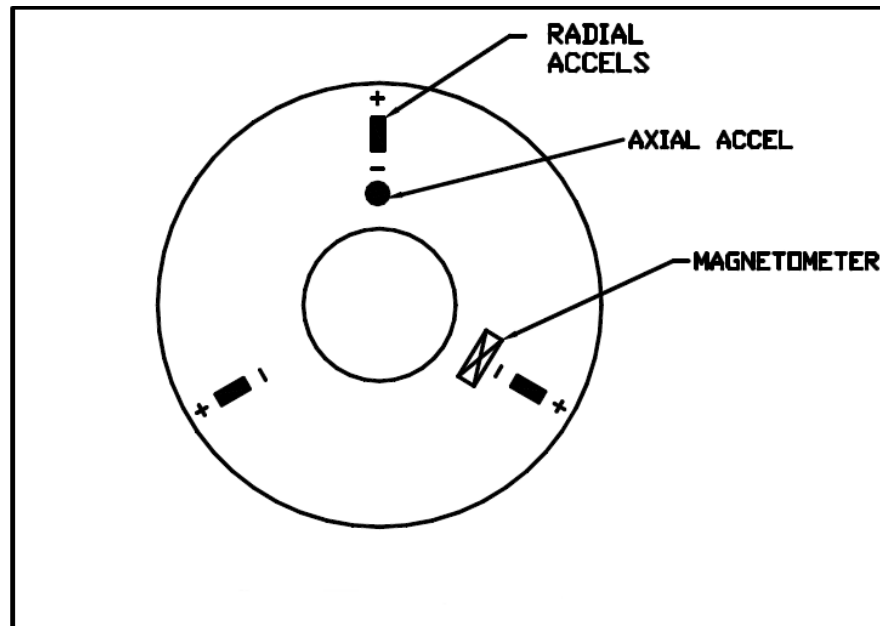
Figure 7 Arrangement of DVMCS Sensors [15]

2.2.6. Bit-Based Data Acquisition System

In 2007, Pastusek, Sullivan and Harris developed a Bit-Based Data Acquisition System and utilized it with the PDC bit[16]. This system is an integrated battery-powered dynamic-behavior sensor and data acquisition module, as shown in

Figure 8. This system was patented in 2010[17]. In this patent, the top view of the system is shown in Figure 9. In this figure, the A1 and A1' are two 5g range accelerometers, and A2 and A2' are two 30g range accelerometers. Meanwhile, the author mentioned that the system may use tri-axial accelerometers or magnetometers instead of on board sensors in the case of plurality.

Figure 8 Assembly Drawing Showing the Approximate Arrangement of the Module Prior to Implantation in the End of a Bit Shank [16]
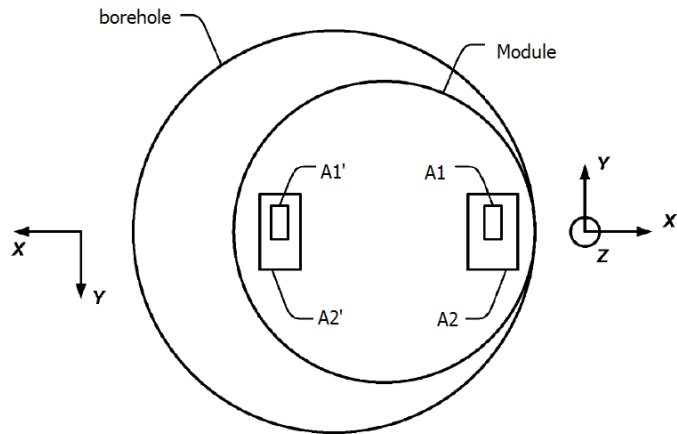
Figure 9 Top View of a Module within a Borehole [17]

2.3. Conclusion

Above all, in laboratory environment, the DAQ system more depends on the sensor and the DAQ module functionality such as the resolution, signal type, signal frequency and so on. Since the DAQ system is designed for different systems and has its designated function, in the Advanced Drilling Laboratory, we should optimize and then apply the design to make the DAQ system more appropriate.

For the downhole measurement tool, the mechanical design is as critical as the electronics. All the downhole measurement tools can survive under harsh downhole environments and function long enough to acquire and store the data during the downhole operation. At the same time, as a result of the limited space downhole, all the devices have to fit in the drill pipe, which is also a challenge. However, downhole measurement tools are based on different algorithms and mechanical designs aiming for their diverse experimental purposes, which asks for a new

algorithm and mechanical design for the Advanced Drilling Laboratory downhole measurement tool.

3. Laboratory System for Measurement of Bit Operating Conditions

3.1. Introduction

Li et al. [2] developed the Small Drilling Simulator (SDS) in 2010 to evaluate the influence of bit vibration on ROP. Figure 10 shows the SDS previous setup when Li did his experiment. After Li, Abtahi et al. [18] utilized the SDS to conduct the bit wear analysis and optimization research. In 2011, Babatunde and Butt [3] added in a flow control system on SDS to conduct the research on Effects of Vibration Frequency on ROP using a PDC bit.
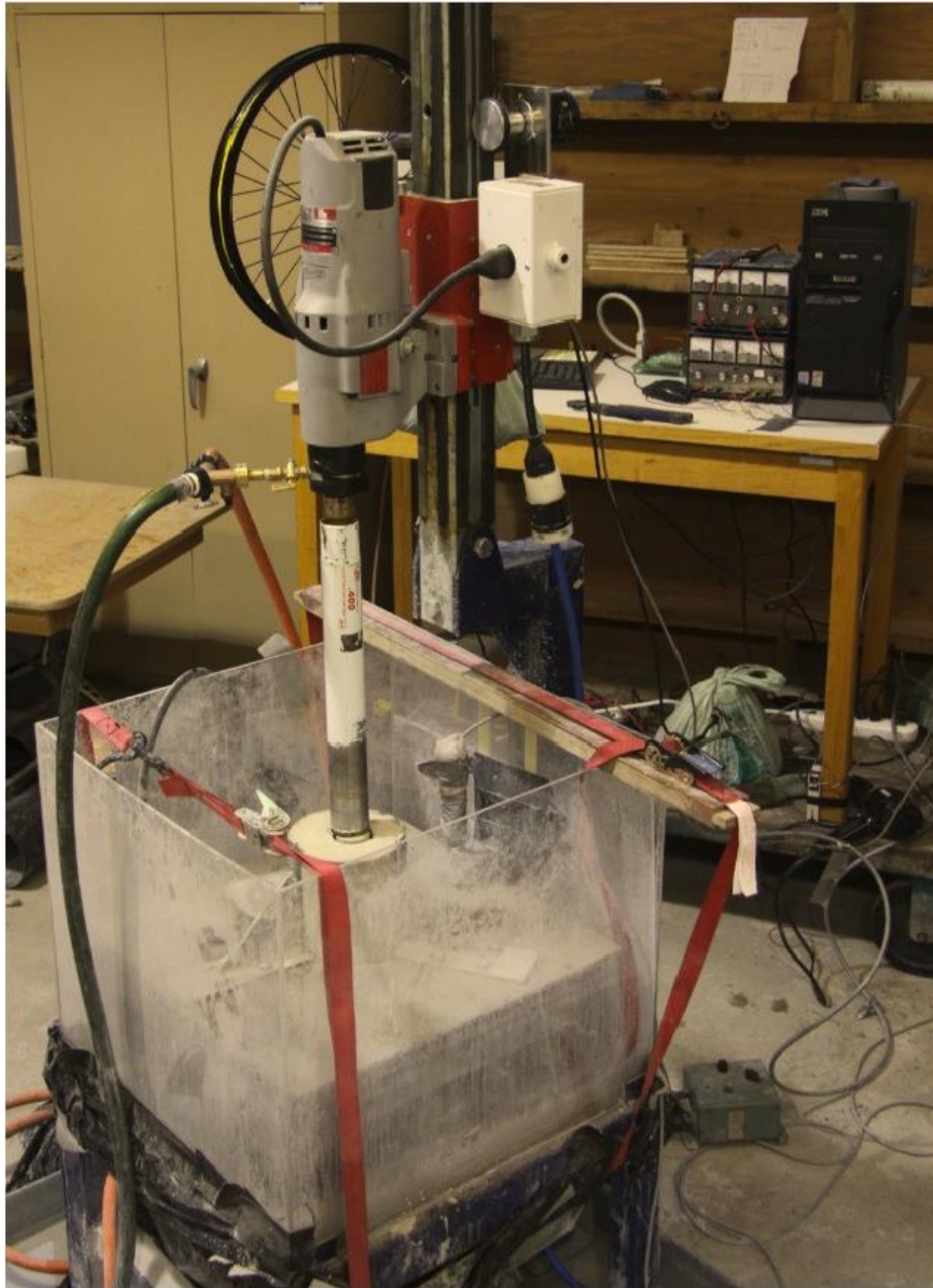
Figure 10 SDS Previous Setup

However, the previous setup only has limited measurements and accuracy is not good. Some new measuring instrumentation and Signal Express software were needed.

At the same time, to improve the safety of the lab operation, a remote control system and emergency stop switches were also added for the system. In spring 2012, a new design of the electrical system was completed. After the system was set up, the system calibration and data validation were implemented. However, the whole system had some electricity noise problems, which will be discussed in this chapter.

The system is built as an integrated DAQ system which can be operated for different experimental purposes with control function inside. The whole system is built with the LabVIEW software and mainly uses the DAQ assistant. This chapter will introduce the system setup and calibration.

3.2. System Setup

3.2.1.   Sensors Setup

The sensors setup is given in Table 1 and includes a load cell, 2 pressure transducers, a flow meter, an LPT, an accelerometer, a rotary encoder, a Hall Effect sensor and a variable frequency drive (VFD) power output.

▪   **Table 1** Summary of SDS Sensors

Sensor	Range	Specifications
Load-cell	2000lbs	Honeywell 3173-2K,0.07 % accuracy, 4-20 mA output
pressure transducer	1500psi	Endress and Hauser PMP131, 24V DC power, 4-20 mA output
pressure transducer	1000psi	GE UNIK 5000, 24V DC power, 4-20 mA output
flow meter	5-50GPM	Omega FTB-1425, 4-20 mA output
LPT	200mm	Sakae 30LP200, 0-10V output
accelerometer	±4g	Crossbow LP series, 0-4V output
rotary encoder	N/A	Nikon RXA1000-22-1A, 5V DC power, pulse signal output
hall effect sensor	0 to ±90A	CLN-50, ±15V DC power, 50mA nominal analog output

3.2.1.1. Load cell setup

The load cell was purchased from Honeywell and the model number is 3173-2K[19], which can take 2000lbs weight and have 0.07 % accuracy. The load cell is connected to the junction box and then an in-line amplifier is used to amplify the signal. After

amplification, the signal is turned into 4-20 mA and one 250 ohm precise resistor is used to convert the signal into 0-5 V, which is easier for the DAQ board to acquire.

The load cell is located below the pressure cell and used to record the force applied on the bit. (Figure 11)

3.2.1.2. Pressure transducer setup 1

The pressure transducer is from Endress and Hauser, the model number is PMP131[20], whose measurement range is 0-1500 psi. The pressure transduce is powered by 24V DC, and the output is 4-20 mA. Then another 250 ohm precise resistor is used to convert the signal into 0-5 V.

The pressure transducer is located near the pump to monitor the pump pressure for safety operation. (Figure 11)

3.2.1.3. Pressure transducer setup 2

The pressure transducer is from GE, the model number is UNIK 5000[21], whose measurement range is 0-1000 psi. The pressure transduce is powered by 7-32V DC. We use 24V in this setup and the output of this sensor is 4-20 mA. And we also use a 250 ohm precise resistor to convert the signal into 0-5 V.

The pressure transducer is located near the pump to monitor the pump pressure for safety operation. (Figure 11)

3.2.1.4. LPT (Linear Potential Transducer) setup

The LPT model number is 30LP200[22], which is from Sakae, and the stroke is 200mm long, which is used to track the travel of the drill string. This LPT was powered up by 10V DC in the previous setup, so here we used 12V instead because 12V is more usual and can be shared with other sensors. The output of LPT is 0-10V and it is very easy for the data acquisition system to acquire.

The LPT is located just below the motor and the motor can move up and down with the drill string. (Figure 11 & 12)

3.2.1.5. Rotary encoder setup

The Rotary encoder is a Nikon Rotary Encoder RXA1000-22-1A, which has three different signal outputs. In the three signal outputs, one is a clockwise counter, one is a counter-clockwise counter, and the other one is the reference counter. In the current setup, due to the port number limitation, only one counter is used and the rotary speed is obtained through the conversion. This rotary encoder is powered up by 5V DC, and its output is a pulse signal, in which the counter in DAQ is used for recording.

The rotary encoder is located beside the shaft of the motor, and is rotary at the same speed with the motor shaft. (Figure 11 & 12)

3.2.1.6. Accelerometer setup

The accelerometer is an LP series accelerometer [23] from Crossbow, which is a three-axis accelerometer. In the current setup, only one axis is used to determine the

axial vibration of the drill string, and the accelerometer is powered by 5V DC. The measuring range is ±4g, and the output signal is 0-4V.

The accelerometer is attached on the motor and used to record the axial vibration. (Figure 11 & 12)

3.2.1.7. Hall Effect sensor setup

The Hall Effect sensor is one closed loop Hall Effect current sensor, whose model number is CLN-50[24]. The sensor is powered up by ±15V DC and the nominal analog output current is 50mA, whose measuring range is 0 to ±90A and nominal current is 50A rms.

This sensor is located in the junction box of the sensors. One power cable of the motor goes through the sensor. The sensor measures the current getting into the motor and the power of the motor can be calculated by the voltage and the current. (Figure 11)

3.2.1.8. Flow meter setup

Omega FTB-1425[25] is used in our setup to monitor the flow rate from the pump; the measuring range is 5-50GPM and can give out pulse signals. The sensor signal gets to a flow rate indicator, and is transferred into a 4-20mA current signal and then converted into 0-5 V signal by using a 250 ohm precise resistor.

The flow meter is located near the pump to record the pump flow rate. (Figure 11)
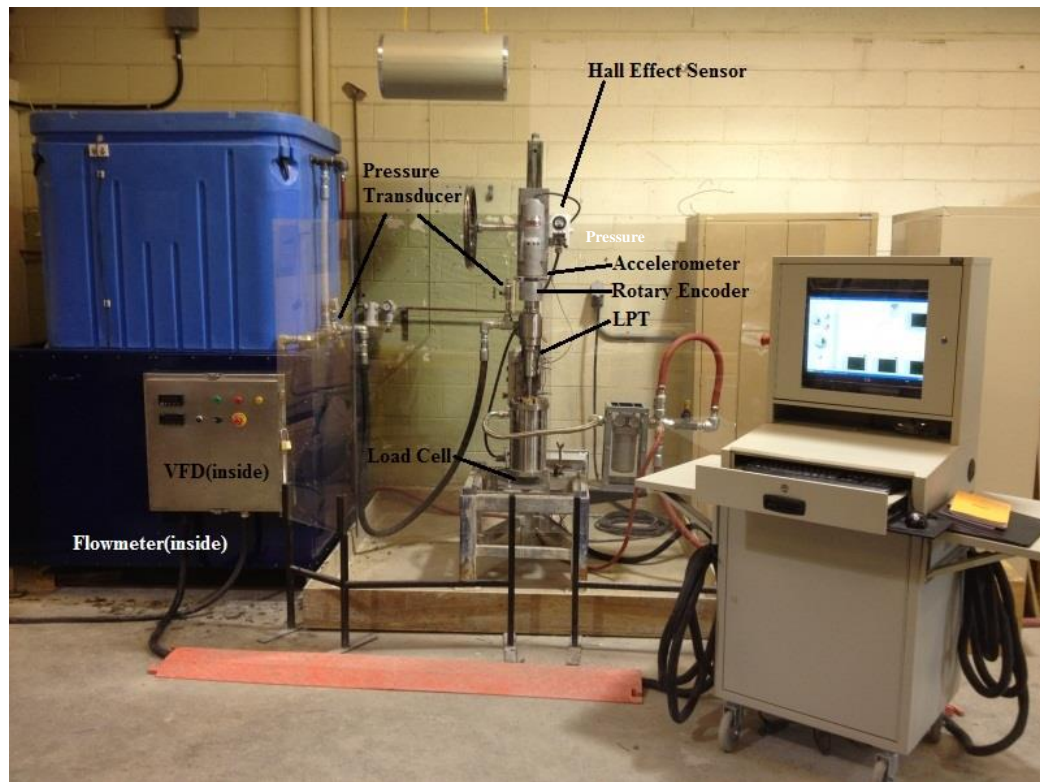
Figure 11 PHASE I setup and sensors locations (Front View)

3.2.1.9. VFD power output

The VFD has a drive that can output a 0-10 V signal indicating the power of the VFD. This signal is used to monitor the power of the VFD. (Figure 11)

3.2.2. Data acquisition setup

This DAQ system utilizes a NI-6024E [26] DAQ Card, which has the capability to capture multiple channel signals in high resolution simultaneously. For our lab usage, the DAQ card is installed on one PC's mainboard aside the SDS drill rig.

The detailed features of NI 6024E are as follows:

• 16 AI channels (eight differentials) with 12-bit resolution

• Two AO channels with 12-bit resolution

• Eight lines of TTL-compatible DIO

• Two 24-bit counter/timers for TIO

• A 68-pin I/O connector

To avoid the aliasing, the DAQ is designed to work at 10 kHz sampling rate, which

is high enough to oversample the sensors data and avoid the aliasing.
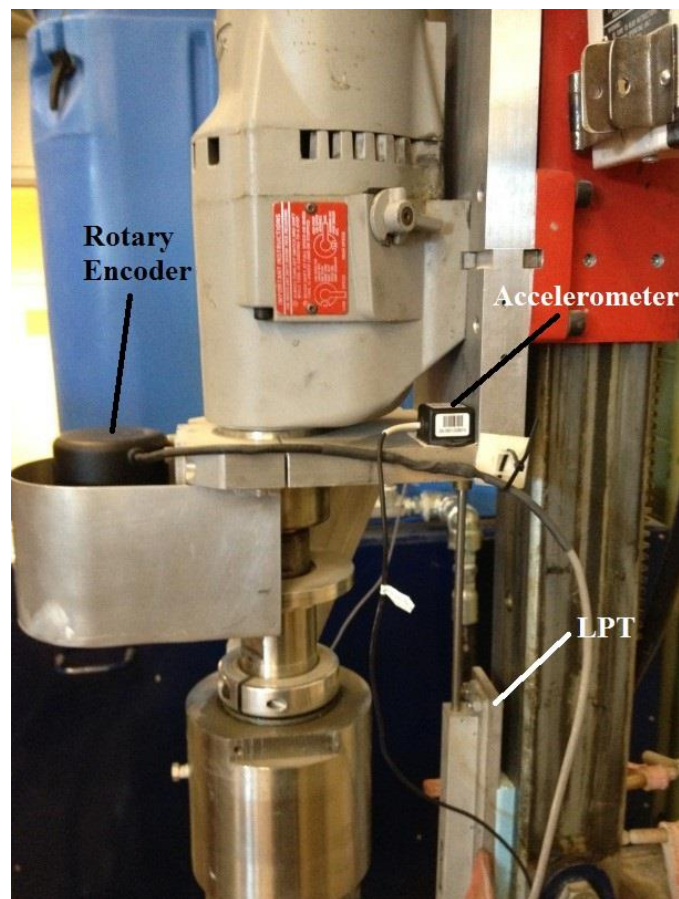
Figure 12 PHASE I Setup and Sensors Locations (Side VIEW)

Based on these features, these eight differential AI channels are used to record the voltage signal input from the above sensors except the rotary encoder, and the signal from the rotary encoder is recorded by one counter/timer.

All the connections from sensors are connected into a 68 Pin I/O connector, and the connection pin diagram is shown in Figure 14.

For different channel input, the LabVIEW software will assign different ports on the 68-pin I/O connector, so the circuit should be connected to the right port.
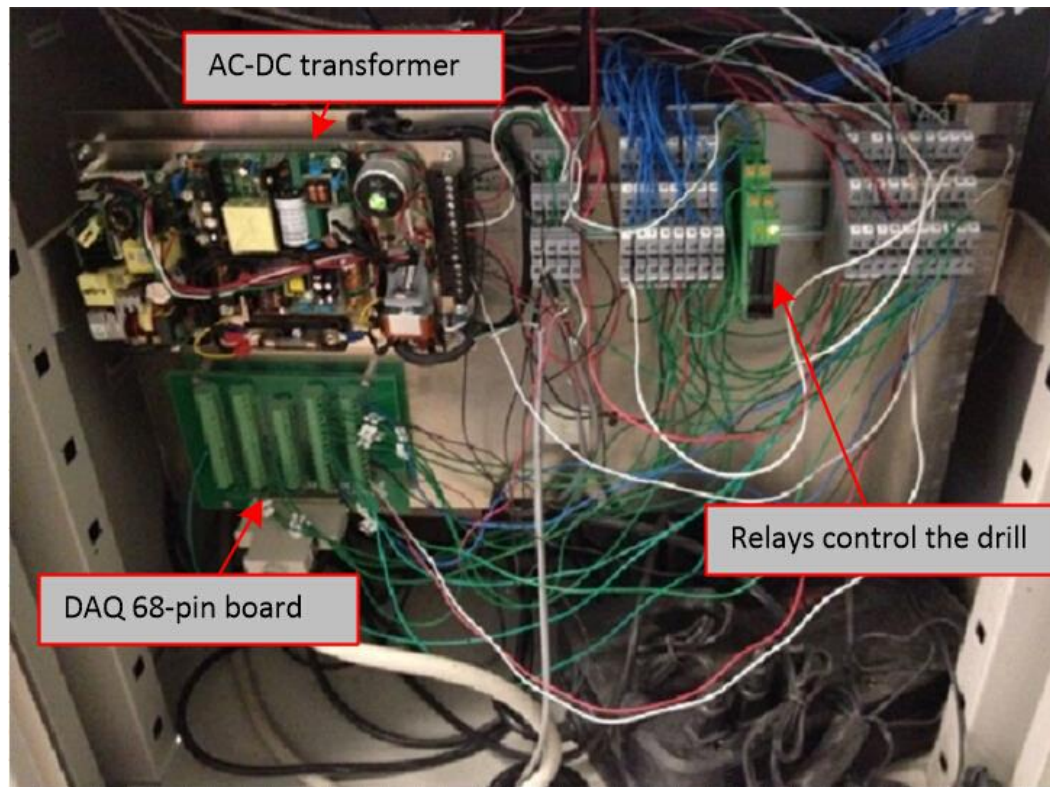
Figure 13 Computer enclosure Wiring and Connection

The next three wiring diagrams will show all the wiring connections and circuit for the computer enclosure (Figure 14), drill rig (Figure 15) and pump station (Figure 16).
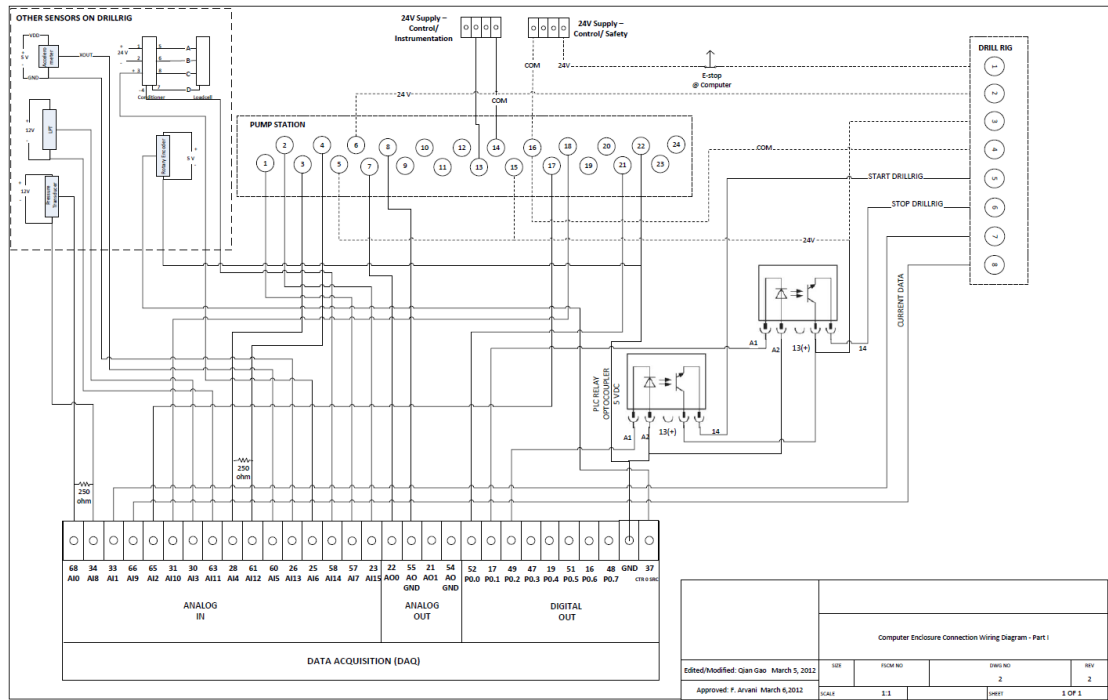
Figure 14 Computer Enclosure Connection Wiring Diagram (Appendix A-9.)

3.2.3. Remote control system setup

This system has a remote control system based on the NI DAQ board Digital output. The board has eight digital outputs, which means that different signals can be used to control different devices. In our setup, one signal is used to operate the pump start and stop, and two signals are used to control the drill start and stop respectively.

3.2.3.1. Pump remote control

The pump remote control is built with a digital relay, in which a digital signal output is used to control the relay on and off, and then control the pump to start and stop.

27
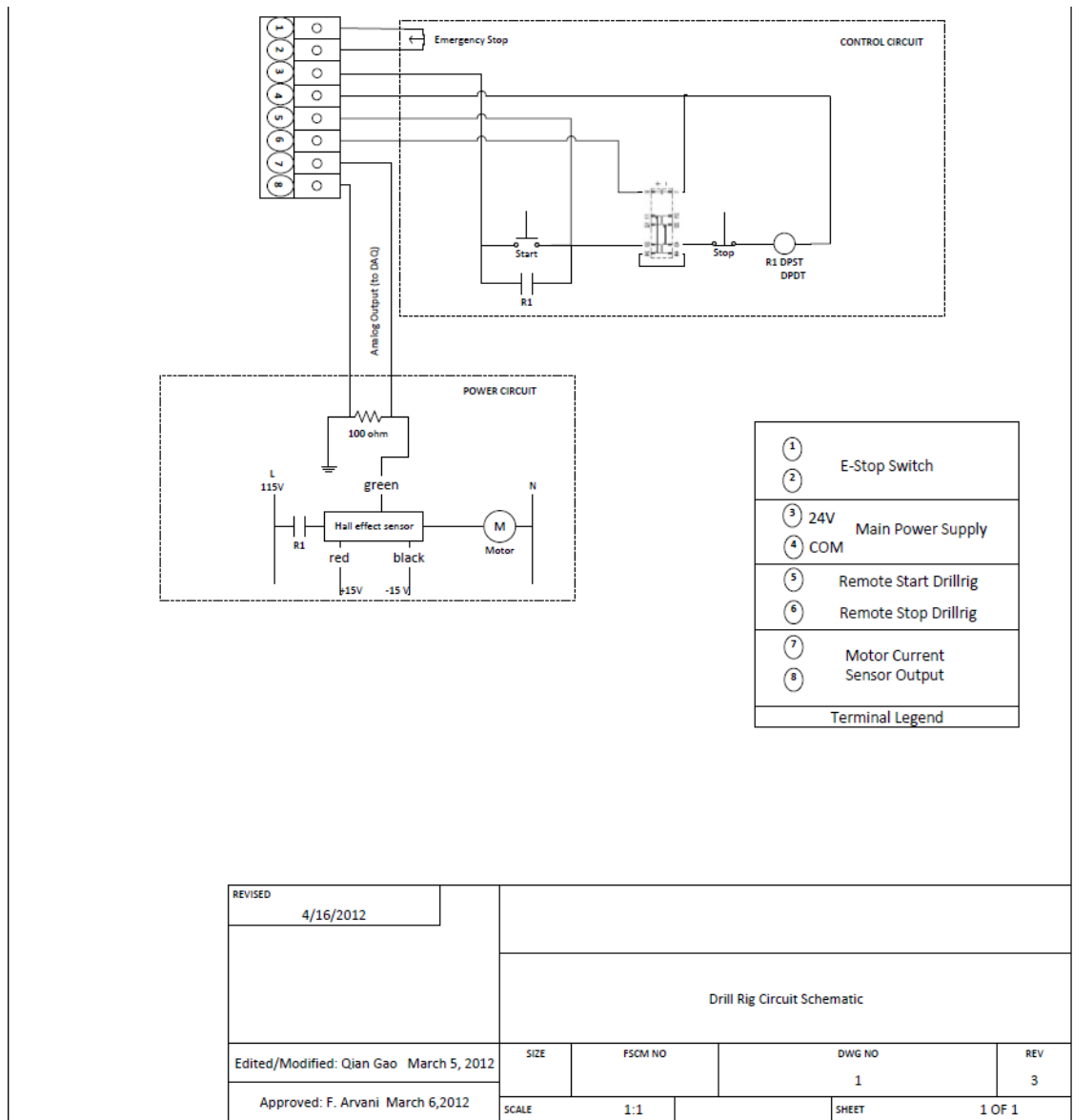
Figure 15 Phase I Drill Rig Connection Diagram (Appendix A-11.)
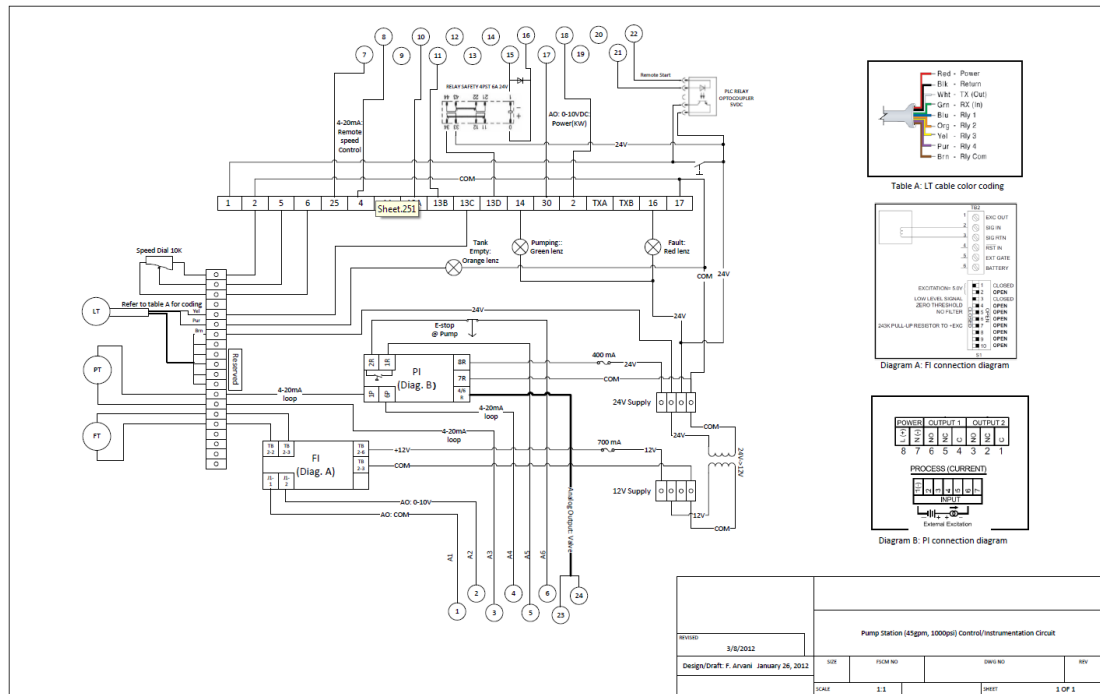
Figure 16 Pump Station Control/Instrumentation Circuit (Appendix A-12.)

3.2.3.2. Drill start and stop remote control

The drill start and stop control also works with relays, but one difference from the pump system is that in this system, two separated relays are used to control the drill, and a latch instead of the switch is used. The designed circuit needs a pulse voltage to excite or stop it, as shown in Figure 13.

3.2.4. User Interface

LabVIEW software is used in current setup. LabVIEW has two panels when designing a project: a front panel and a block diagram. The front panel is for people who operate the system, and the block diagram contains all the device connection, data processing and signal output.

The Figure 17 shows the front panel and Figure 18 shows the block diagram
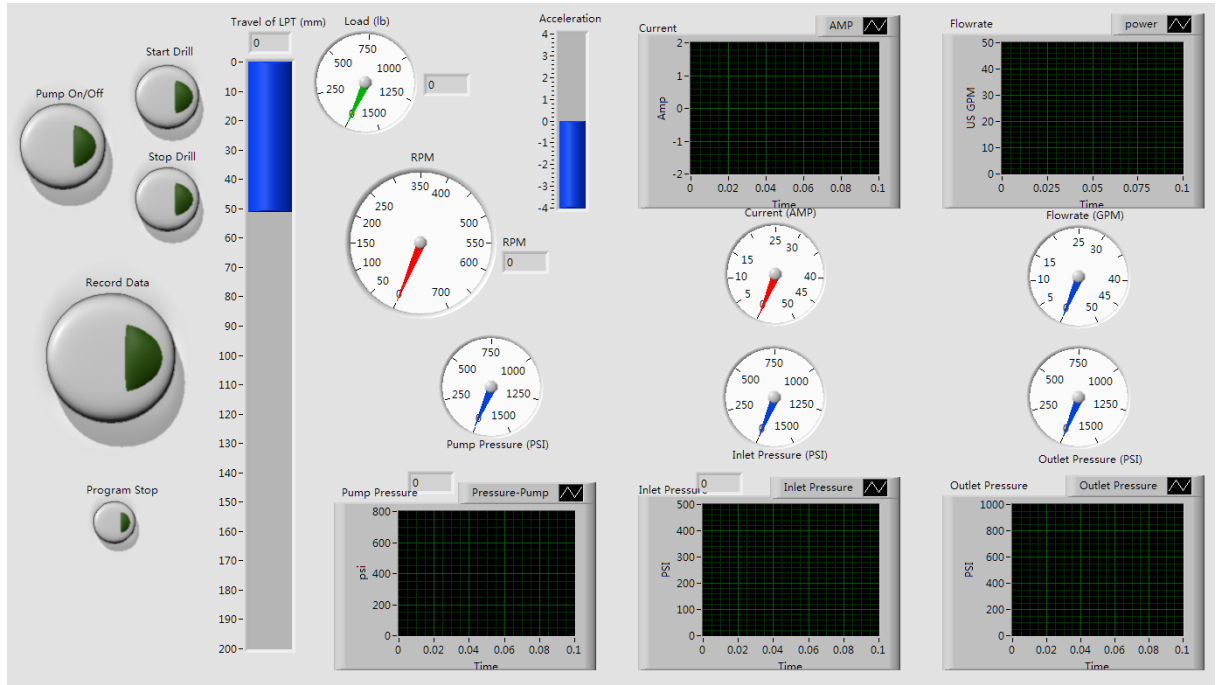
Figure 17 Front Panel for LabVIEW
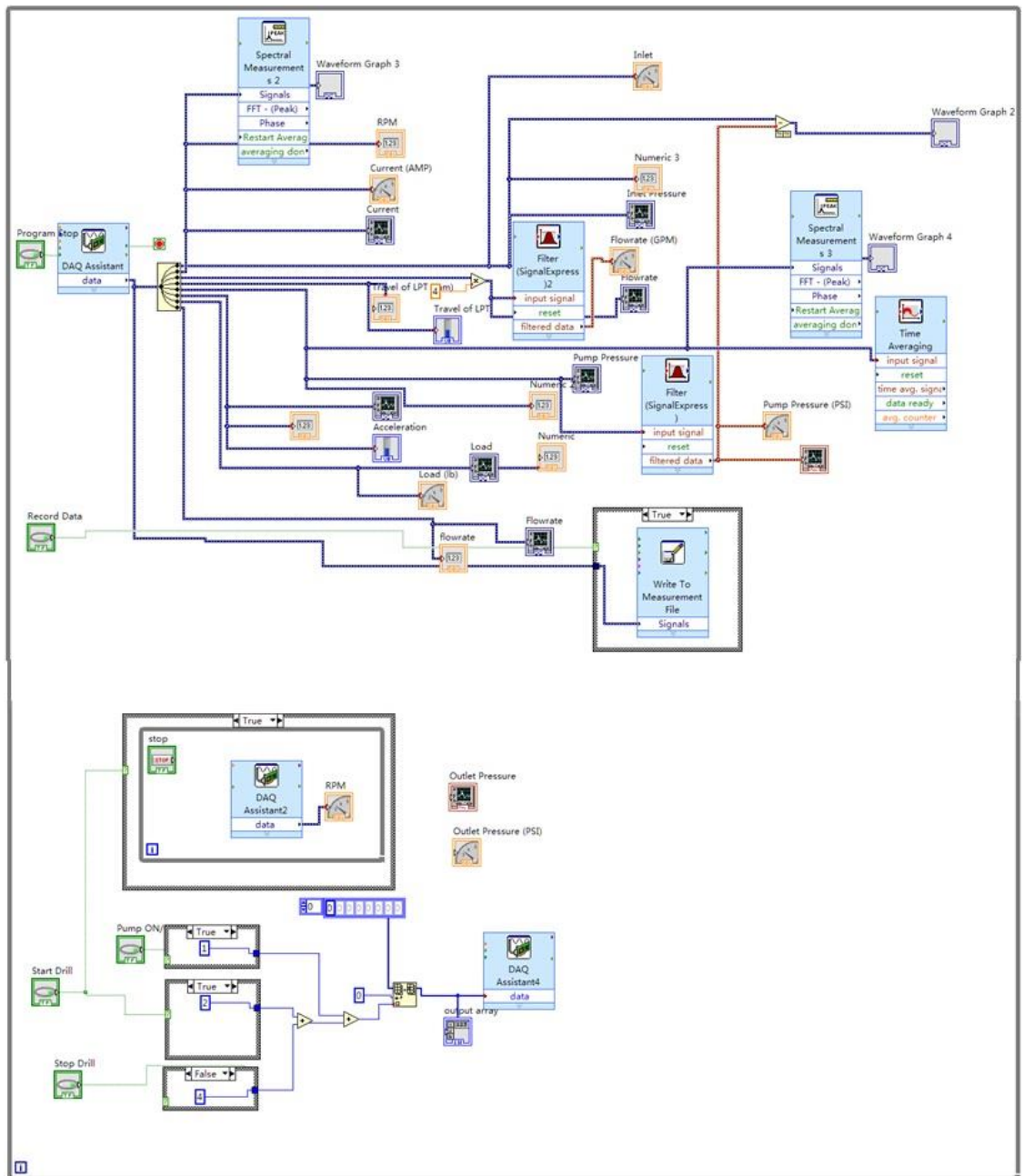
Figure 18 Block Diagram for LabVIEW

3.3. Development Issues and solutions

3.3.1. Noise

Noise always exists in a data acquisition system. During the current system development, there was a very obvious interfering signal which was not usual noise. This signal had much larger amplitude compared to the usable signal and mainly existed in the pressure measurement.

Through discussion and analysis, the source of the signal was determined to be the pump, which creates pressure pulses during rotation. This might cause the reading on the flow meter and pressure transducer to be unstable, but this effect can be minimized by averaging the data.

3.3.2. Hall Effect Sensor

In the circuit design phase, the Hall Effect sensor had a ±15V DC power supply with a 0V reference, which was considered as ground. This assumption led to an unusable result. The signal acquired in the computer did not match the operation of the motor and in order to solve this problem, the 0V reference was connected to the ground.

3.3.3. Rotary Encoder

The rotary encoder is unreliable in this setup, because it can be damaged if subjected to jolts. The photo eye in the sensor impacts the disc and damages itself. The photoelectric sensing of rotation directly generated from the shaft might be a good

choice for setup under severe vibration. The recommended solution is to use a laser sensor mounted on an isolated frame to measure the rotary speed.

3.4. SDS DAQ System Extension (Mobile DAQ System)

In 2012, a field trial testing was scheduled which requires accurate measurements like SDS could provide. A portable system was needed with the capacity to conduct data recording for different sensors, also able to function in various field operation environments.

On account of these reasons, a mobile DAQ system was built in the summer of 2012. This system is also based on LabVIEW but only utilized the Signal Express module for the data acquisition. The actual system is shown in Figure 19. As shown in the figure, the whole system was divided into two parts, one for the power supply and the other for the DAQ system. The two parts were separately installed in two Pelican watertight protective cases, which are able to be carried in any kinds of field environment.

Figure 19 Mobile Power System (Upper) and Mobile DAQ System (Lower)

3.4.1.   Mobile Power System

The Mobile Power System is designed as water-proof when sealed and water-resistant when the top is opened. It is powered by 110V input, and has three different voltage outputs for common analog sensors, which are 5V, 9-12V and 24V respectively. They all generate linear voltage output and we set the 9-12V channel to 10V for current usage. All the connections in the system are mil-spec, which are made from tough material and water-proof, as shown in Figure 20. Since the power system generated heat while running, fans and vents are necessary. However, this changed the water-proof grading from water-proof to water-resistant. Moreover, the entire system is mounted on the panel, which implies that they are all off bottom, so it will help in case some water gets in.

Figure 20 Mobile Power System Front Panel

The power will connect to the DAQ case with a customized cable through DC OUTPUT, as shown in Figure 20.

3.4.2.   Mobile DAQ System

The DAQ system is designed as water-proof. It has an NI9188 Chassis built in and two high resolution DAQ modules NI9237 (24-bit) and NI9205 (16-bit) for acquiring the data from different sensors. In order to avoid the aliasing, the DAQ was designed to work at a high frequency sampling rate-10 kHz, which would oversample the sensors data. The DAQ modules are shown in Figure 21.
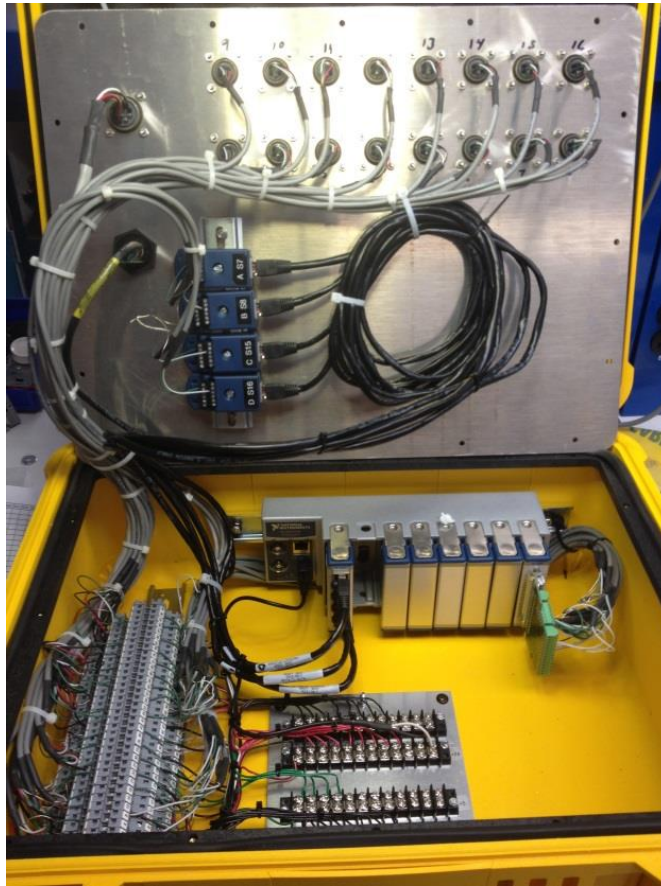
Figure 21 Connections in mobile DAQ system

The DAQ system is capable of working with up to 16 sensors. As labeled in Figure 22, plugs 1,2,3,4,9,10,11,12 are for 24V sensors, and they can support 8 sensors in total; plugs 5,6,13,14 are for 5V sensors; plugs 7,8,15,16 are for 10V sensors, which are specifically designed for load cells in our system.

For one field configuration, Plug 1 is the 4000 psi pressure transducer, plug 2 is the 1500psi pressure transducer, and plug 3 is the flow meter. Plugs 7, 8, and 15 are used respectively for our load cells.

The PC-DAQ is the Ethernet port for data communication with the laptop, as shown in Figure 22

Figure 22 Mobile DAQ System Front Panel

With the caps shown in Figure 22, the Mobile DAQ System is water-proof even when the lid is open. In Figure 23, there are no caps on the front panel, and the mil-spec connection is on the left of the figure, which are waterproof when connected. The PC-DAQ connection is also waterproof, which can transmit the data to the laptop in real-time.

Figure 23 Cable Connection and Mobile DAQ System Front Panel without Caps

3.5. Experiments Summary

This drilling setup was used in a laboratory environment in which the need of accurate measurement of operational variables changes with each experimental setup. The LabVIEW software is ideal for this setup as this software allows the sensor system to be integrated with the control of the equipment. It also allows for the development of these systems in a modular way, as well as testing and troubleshooting on individual components without affecting the system as a whole.

Since the SDS was setup, it starts to serve the group member in different experiments. Khorshidian et al. [27] used the SDS to measure water flow rate, WOB and BHP. Pronin[4] used the SDS to finish his pulse-cavitation tool prototype testing. Figure 24 shows one example form Pronin [4], which measures the inlet pressure and outlet

pressure of the pulse-cavitation tool at a high frequency indicating that the pulse-cavitation tool generates pressure pulses as predicted.
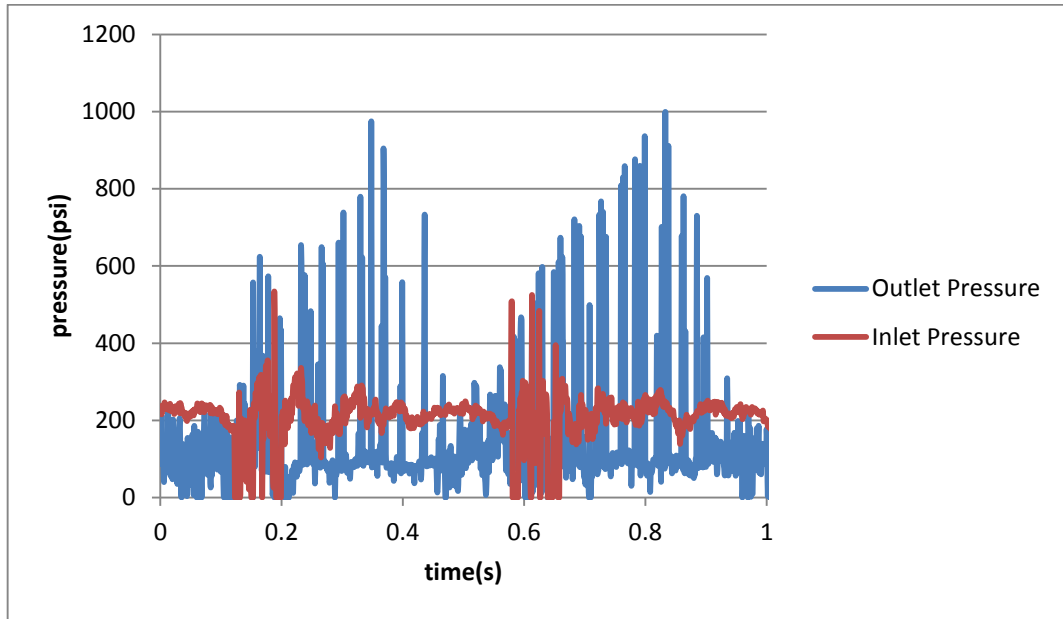
Figure 24 Pressure pulsations from Pronin [4]

Figure 25 shows the data from SDS system which measures the vibration generated by the pulse-cavitation tool [4].
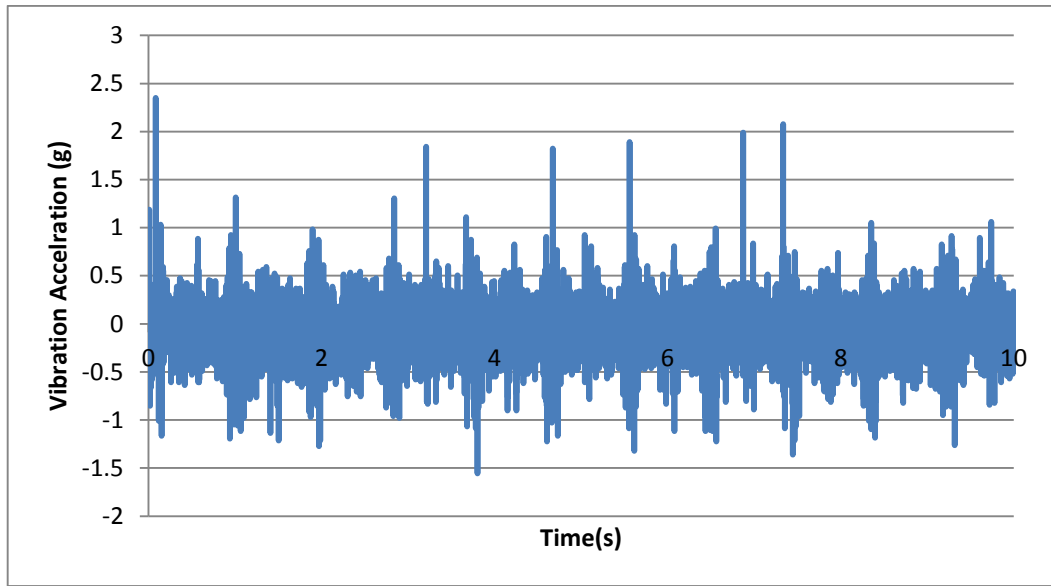
Figure 25 Vibration measurement for Pulse Cavitation tool [4]

For the Mobile DAQ system, Babapour [5] completed his experiment on Active-VARD Tool and pulse cavitation tool. The figure below shows the pressure pattern vs different flow rate from pulse cavitation tool experiment. All these data were collected by utilizing the Mobile DAQ system.
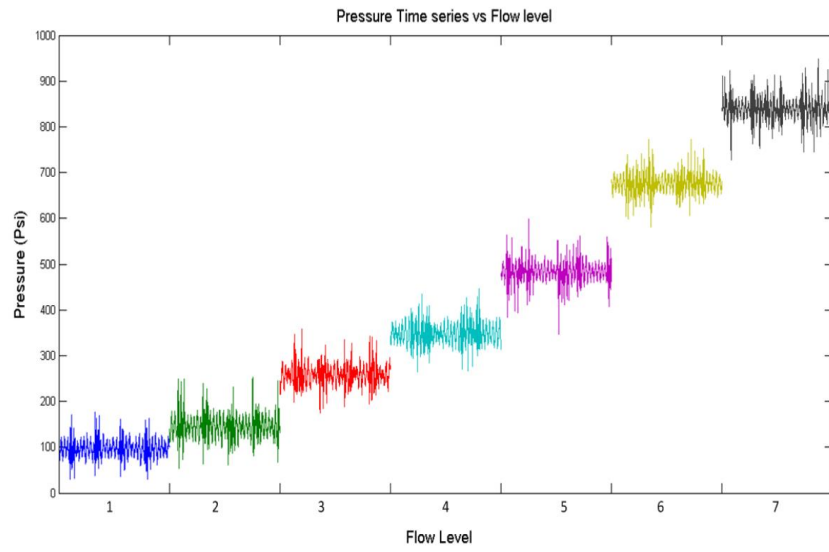
Figure 26 Drilling pipe pressure versus flow level in Babapour's test [5]

4. Down-Hole Measurement Tool (Sensor Sub)

As stated earlier, downhole bit and drill string motions were needed for a variety of experimental requirements, including VARD tool evaluation, drill string motion measurement, and Seismic While Drilling (SWD) source characterization. The design of these tools requires down-hole axial, lateral, tangential vibration and rotatory speed measurement. For this reason, three accelerometers and one magnetometer were selected. For data acquisition and recording, an onboard recording unit utilizing a micro-SD card was installed in the measurement tool.

4.1. Background

The Advanced Drilling Laboratory conducted a field trial in September 2014 to evaluate the VARD technology under field conditions. Because the commercial drilling tool (black box) for down-hole data recording can only give out the data after an internal process (which normally involves providing average or RMS values over set periods of time), it cannot be used in experiments or drilling field trials. Therefore, a down-hole measurement tool (Sensor Sub) was needed to record the down-hole vibration with high sampling rate.

4.2. Design Methodology

The basic down-hole measurement tool (Sensor Sub) sensor model comprises of four spaced tri-axial accelerometers positioned within the wall of a measurement tool section. Three of these four accelerometers cooperate and interact with each other to

measure the longitudinal, lateral and torsional vibrations. The fourth accelerometer measures shocks.

Several possible configurations of the basic sensor arrangements described above are feasible. The first configuration of a vibration monitoring system [28] is shown in Figure 27, and the schematic diagram is shown as a cross-section of a drill segment with an interior longitudinal opening and a drill collar wall. Four accelerometers are shown within the wall of drill collar section. Three accelerometers are schematically identified by the rectangular box and identified by A1, A2 and A3. These three accelerometers are positioned 120° apart from one another and are also positioned to measure tangential acceleration forces on the outer circumference of drill collar. Accelerometer A1 is positioned on a reference plane (0°/360°). The measurement of tangential forces is indicated by the tangential lines.
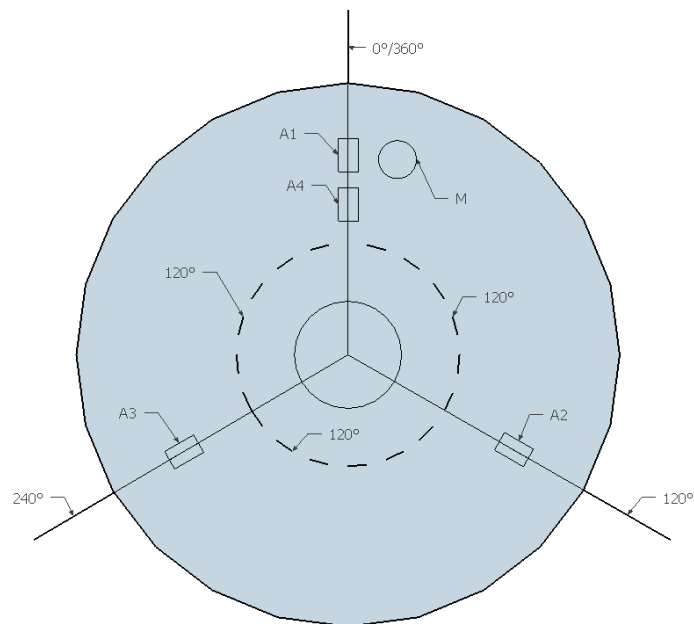
Figure 27 Layout of Sensors in Drill Collar (Configuration 1)

In accordance with the layout, the following equations are utilized to measure the torsional vibration (Equation 1), lateral vibration (for a given angle) (Equation 2) and maximum lateral vibration angle (Equation 3) [28].

$$A_{\tau 0} = \frac{A_1 + A_2 + A_3}{3} \tag{1}$$

$$A_{L\alpha} = \frac{1}{3}\left(\frac{A_1 - A_{\tau 0}}{sin(-\alpha)} + \frac{A_2 - A_{\tau 0}}{sin(120 - \alpha)} + \frac{A_3 - A_{\tau 0}}{sin(240 - \alpha)}\right) \tag{2}$$

$$\alpha_{max} = tan^{-1}\left(\frac{A_1 * cos(90) + A_2 * cos(210) + A_3 * cos(330)}{A_1 * sin(90) + A_2 * sin(210) + A_3 * sin(330)}\right) \tag{3}$$

In equation 2, when α equals 0, 120, 240, the friction which has a denominator equals 0 is meaning nothing and will be consider as 0 during calculation.

This method will get torsion vibration and also lateral vibration, but there is another thought about it. Because the measurement tool is going to take torque higher than 5000 lb ft, placing the accelerometers l20 ° apart from one another will reduce the material in between. Since we would like to have a package of sensors for easy installation, this means that the sensors in this layout will take more than 240 ° space and leave only 1/3 material to take torque. For safety concern, this design was modified into Sensor Configuration 2, which is shown in Figure 28.

In Sensor Configuration 2, we place accelerometer A2 in an opposite position, which is going to give an inverse measurement in torsional vibration and also lateral vibration. To approach better results, we are using tri-axial accelerometers instead of uniaxial accelerometers in this configuration. In this arrangement, the tri-axial accelerometers give the lateral vibration and torsional vibration simultaneously. Thus, the complexity is reduced further.
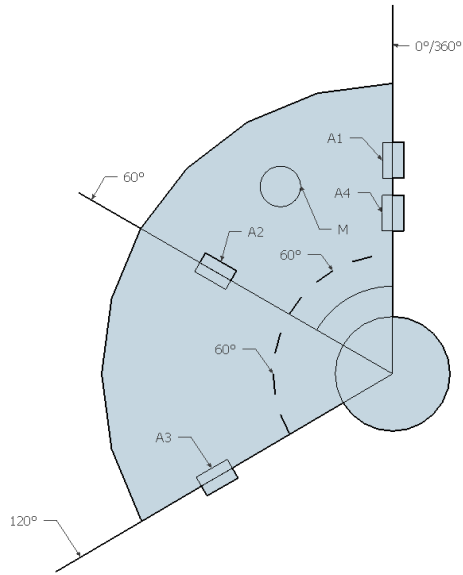
Figure 28 Layout of Sensors in Drill Collar (Method 2)

A further sensor simplification can be done by placing two accelerometers in 90°
and thus calculating torsional and lateral vibration in the Cartesian coordinate system.
A3 is only used for axial acceleration. This Sensor Configuration 3 is shown in Figure
29.
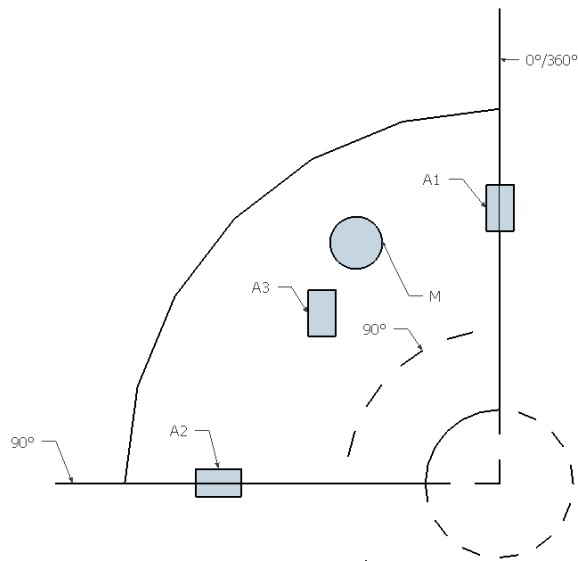
Figure 29 Layout of Sensors in Drill Collar (Method 3)

4.2.1. Tool Face Angle, Inclination and Azimuth

In the system we have three accelerometers and one magnetometer, and they are all tri-axial sensors. The outputs are shown below:

$$\mathbf{A1} = \begin{pmatrix} a1x \\ a1y \\ a1z \end{pmatrix} \quad \mathbf{A2} = \begin{pmatrix} a2x \\ a2y \\ a2z \end{pmatrix} \quad \mathbf{A3} = \begin{pmatrix} a3x \\ a3y \\ a3z \end{pmatrix} \quad \mathbf{M} = \begin{pmatrix} mx \\ my \\ mz \end{pmatrix} \tag{4}$$

The locations of the sensors in design are shown below:
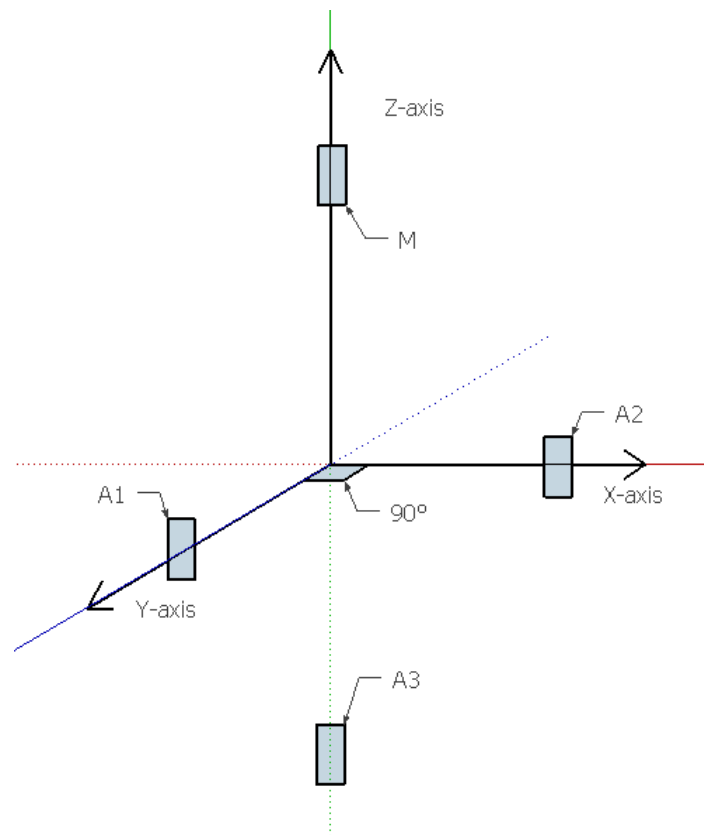
Figure 30 3D location of sensors

In order to get the bit vibration, A1 and A2 are the sensors which provide the normal operation data. They both have a 4g range and the sensors are located 90° apart.
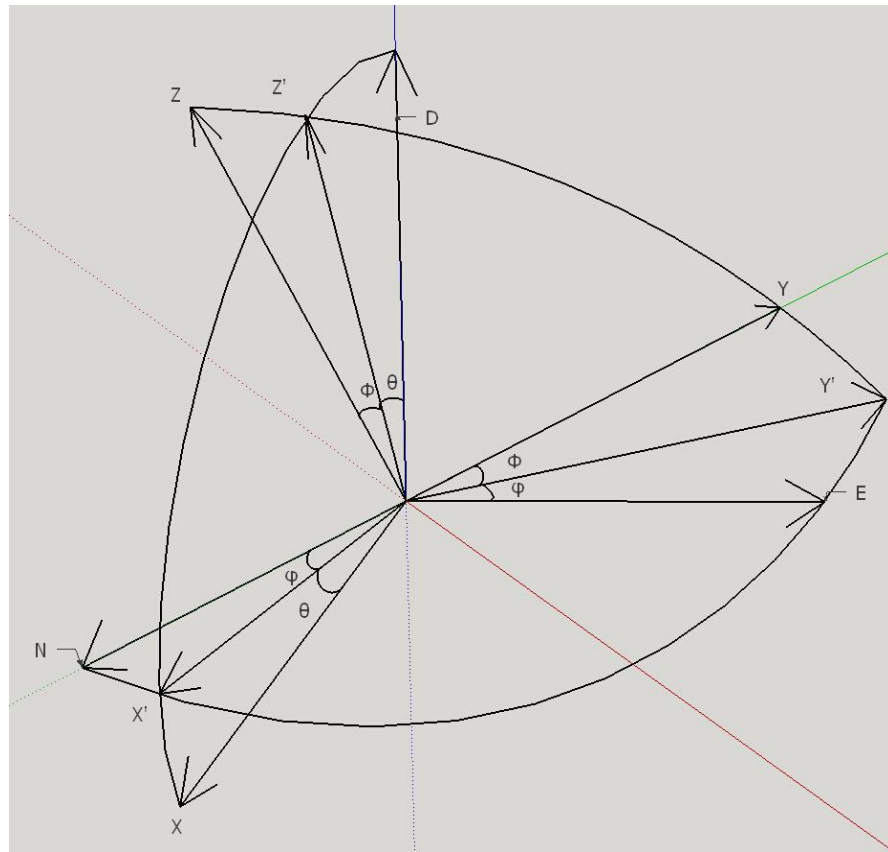
Figure 31 Sketch of Transformation of Coordinate System

According to the rotation transformation of Euler's theorem, carrier posture in the space is only available for a limited time relative to the geographical coordinating system rotation.

At beginning, the sensors' coordinates (X-Y-Z) are the same as the NED (north-east-down) coordinates (N-X, E-Y, D-Z). Then revolving around the D axis by φ degree, we will get X'Y'D coordinates, revolving around Y' axis θ degree, we will get XY'Z' coordinates and revolving around X axis ∅ degree, we will get the current position XYZ coordinates.

Each revolution involves a coordinate transformation. It can be represented by a matrix transformation.

$$R_\varphi = \begin{pmatrix} cos\varphi & sin\varphi & 0 \\ -sin\varphi & cos\varphi & 0 \\ 0 & 0 & 1 \end{pmatrix} R_\theta = \begin{pmatrix} cos\theta & 0 & -sin\theta \\ 0 & 1 & 0 \\ sin\theta & 0 & cos\theta \end{pmatrix}$$

$$R_\emptyset = \begin{pmatrix} 1 & 0 & 0 \\ 0 & cos\emptyset & sin\emptyset \\ 0 & -sin\emptyset & cos\emptyset \end{pmatrix} \qquad (5)$$

So the sensors coordinate have the following relationship with NED coordinate.

$$\mathbf{U}_{XYZ} = \mathbf{R}_\emptyset \mathbf{R}_\theta \mathbf{R}_\varphi \mathbf{U}_{NED} \qquad (6)$$

$$\mathbf{R}_\varphi{}^T \mathbf{R}_\theta{}^T \mathbf{R}_\emptyset{}^T \mathbf{U}_{XYZ} = \mathbf{U}_{NED} \qquad (7)$$

In our setup, the accelerometer A3 has results

$$\mathbf{A3} = \begin{pmatrix} a3x \\ a3y \\ a3z \end{pmatrix} \qquad (8)$$

$$\begin{pmatrix} a3x \\ a3y \\ a3z \end{pmatrix} = \mathbf{R}_\emptyset \mathbf{R}_\theta \mathbf{R}_\varphi \begin{pmatrix} 0 \\ 0 \\ g \end{pmatrix} \qquad (9)$$

g is the local gravitational acceleration, $g = 9.81\text{ms}^{-2}$, and to do an inverse pitch and roll,

$$\mathbf{R}_\theta{}^T \mathbf{R}_\emptyset{}^T \begin{pmatrix} a3x \\ a3y \\ a3z \end{pmatrix} = \mathbf{R}_\varphi \begin{pmatrix} 0 \\ 0 \\ g \end{pmatrix} \qquad (10)$$

$$\begin{pmatrix} cos\theta & 0 & sin\theta \\ 0 & 1 & 0 \\ -sin\theta & 0 & cos\theta \end{pmatrix} \begin{pmatrix} 1 & 0 & 0 \\ 0 & cos\emptyset & -sin\emptyset \\ 0 & sin\emptyset & cos\emptyset \end{pmatrix} \begin{pmatrix} a3x \\ a3y \\ a3z \end{pmatrix} = \mathbf{R}_\varphi \begin{pmatrix} 0 \\ 0 \\ g \end{pmatrix} \qquad (11)$$

$$\begin{pmatrix} cos\theta & sin\theta sin\emptyset & sin\theta cos\emptyset \\ 0 & cos\emptyset & -sin\emptyset \\ -sin\theta & sin\emptyset cos\theta & cos\theta cos\emptyset \end{pmatrix} \begin{pmatrix} a3x \\ a3y \\ a3z \end{pmatrix} = \mathbf{R}_\varphi \begin{pmatrix} 0 \\ 0 \\ g \end{pmatrix} \qquad (12)$$

The y component defines the tool face (roll) angle $\emptyset$ as

$$a3ycos\emptyset - a3zsin\emptyset = 0 \tag{13}$$

$$tan\emptyset = \frac{a3y}{a3z} \tag{14}$$

The x component gives the inclination (pitch) angle θ as

$$a3xcos\theta + a3ysin\theta sin\emptyset + a3zsin\theta cos\emptyset = 0 \tag{15}$$

$$a3x + a3ytan\theta sin\emptyset + a3ztan\theta cos\emptyset = 0 \tag{16}$$

$$tan\theta = -\frac{a3x}{a3ysin\emptyset + a3zcos\emptyset} \tag{17}$$

Since the angle θ and $\emptyset$ are known from the accelerometer, the magnetometer can give the orientation of the facing.

In the earth's magnetic field, the angle of inclination of the geomagnetic field measures downwards from horizontal and varies over the earth's surface from $-90°$ at the south magnetic pole through $0°$ near the equator to $+90°$ at the north magnetic pole. Use δ to denote. More detailed geomagnetic field maps can be obtained from the *World Data Center* for Geomagnetism[29].

In addition, the geomagnetic field doesn't have a point to east component, so the earth magnetic field can be denoted as $\begin{pmatrix} Bcos\delta \\ 0 \\ Bsin\delta \end{pmatrix}$

$$\mathbf{R}_\theta{}^T\mathbf{R}_\emptyset{}^T\begin{pmatrix} mx \\ my \\ mz \end{pmatrix} = \mathbf{R}_\varphi\begin{pmatrix} Bcos\delta \\ 0 \\ Bsin\delta \end{pmatrix} \tag{18}$$

$$\begin{pmatrix} cos\theta & 0 & sin\theta \\ 0 & 1 & 0 \\ -sin\theta & 0 & cos\theta \end{pmatrix} \begin{pmatrix} 1 & 0 & 0 \\ 0 & cos\emptyset & -sin\emptyset \\ 0 & sin\emptyset & cos\emptyset \end{pmatrix} \begin{pmatrix} mx \\ my \\ mz \end{pmatrix}$$

$$= \begin{pmatrix} cos\varphi & sin\varphi & 0 \\ -sin\varphi & cos\varphi & 0 \\ 0 & 0 & 1 \end{pmatrix} \begin{pmatrix} Bcos\delta \\ 0 \\ Bsin\delta \end{pmatrix} \qquad (19)$$

$$\begin{pmatrix} cos\theta & sin\theta sin\emptyset & sin\theta cos\emptyset \\ 0 & cos\emptyset & -sin\emptyset \\ -sin\theta & sin\emptyset cos\theta & cos\theta cos\emptyset \end{pmatrix} \begin{pmatrix} mx \\ my \\ mz \end{pmatrix} = \begin{pmatrix} Bcos\delta cos\varphi \\ -Bcos\delta sin\varphi \\ Bsin\delta \end{pmatrix} \qquad (20)$$

$$\begin{pmatrix} cos\theta mx + sin\theta sin\emptyset my + sin\theta cos\emptyset mz \\ cos\emptyset my - sin\emptyset mz \\ -sin\theta mx + sin\emptyset cos\theta my + cos\theta cos\emptyset mz \end{pmatrix} = \begin{pmatrix} Bcos\delta cos\varphi \\ -Bcos\delta sin\varphi \\ Bsin\delta \end{pmatrix}$$

$$= \begin{pmatrix} Bx \\ By \\ Bz \end{pmatrix} \qquad (21)$$

This $\begin{pmatrix} Bx \\ By \\ Bz \end{pmatrix}$ represents the components of the magnetometer sensors after

de-rotating to the flat plane with $\theta = \emptyset = 0$

$$Bx = Bcos\delta cos\varphi \qquad (22)$$

$$By = -Bcos\delta sin\varphi \qquad (23)$$

We can get $tan\varphi$

$$tan\varphi = \frac{By}{Bx} = \frac{cos\emptyset my - sin\emptyset mz}{cos\theta mx + sin\theta sin\emptyset my + sin\theta cos\emptyset mz} \qquad (24)$$

Azimuth φ can be calculated by

$$\varphi = \frac{180}{\pi} * tan\varphi + D \qquad (25)$$

The declination (D) is the angle between the geographic North and the horizontal

component. D = +1.367 is an example value.

If φ< 0, then add 360° to φ; if φ > 360°, then subtract 360° from φ.

4.2.2. Axial Vibration and Shocks

The axial vibration (the vibration along the drill string) can be obtained from

$$A_a = \frac{a1z + a2z}{2} \tag{26}$$

If shock happens, then $A_a = a3z$

4.2.3. Angular Velocity and Stick-Slip

From φ value, we can get angular velocity ω.

$$\omega = \frac{\Delta\varphi}{\Delta t} \tag{27}$$

Stick-slip can be observed from ω values. One sudden decrease along with a sudden increase of ω will indicate that a stick-slip happened at the bit.

4.2.4. Lateral Vibration
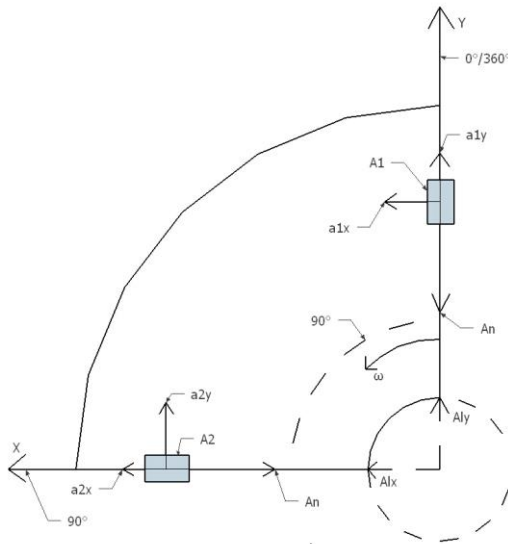
Figure 32 Decomposition of Accelerations

$$a1x = \alpha * r + A_{lx} \qquad (28)$$

$$a2x = A_{lx} - A_n \qquad (29)$$

$$a1y = A_{ly} - A_n \qquad (30)$$

$$a2y = A_{ly} - \alpha * r \qquad (31)$$

In the above equations, $\alpha, r, A_{lx}, A_{ly}, A_n$ are angular acceleration, direction of accelerometer from center, lateral vibration in x-axis direction, lateral vibration in y-axis direction, and centripetal acceleration, respectively.

From equation 28 and 31, we can get

$$a1x + a2y = A_{lx} + A_{ly} \qquad (32)$$

From equation 29 and 30, we can get

$$a2x - a1y = A_{lx} - A_{ly} \qquad (33)$$

From equation 32 and 33, we can get from

$$A_{lx} = \frac{a1x + a2y + a2x - a1y}{2} \qquad (34)$$

$$A_{ly} = \frac{a1x + a2y - a2x + a1y}{2} \qquad (35)$$

After we calculated the two components of lateral vibration, the maximum lateral acceleration can be obtained from

$$A_l = \sqrt{A_{lx}^2 + A_{ly}^2} \qquad (36)$$

If we set the angle between the direction of maximum lateral vibration (vibration perpendicular to the drill string) and X-axis is β.

The direction of maximum lateral vibration is

$$\beta = tan^{-1}\left(\frac{A_{ly}}{A_{lx}}\right) \qquad (37)$$

4.2.5. Torsional Vibration

From equation 28 to equation 31, we can back calculate $\alpha * r$, which is tangential

acceleration calculated from angular acceleration and radius

$$\alpha * r = \frac{a1x - a2y - a2x + a1y}{2} \qquad (38)$$

4.2.6. Whirl

The identification of whirl can be done by using a cross plot of the lateral

acceleration signals. Figure 33 shows the X and Y axial lateral acceleration cross plots.

The test result can be compared with the figures to identify whether the whirl happened.
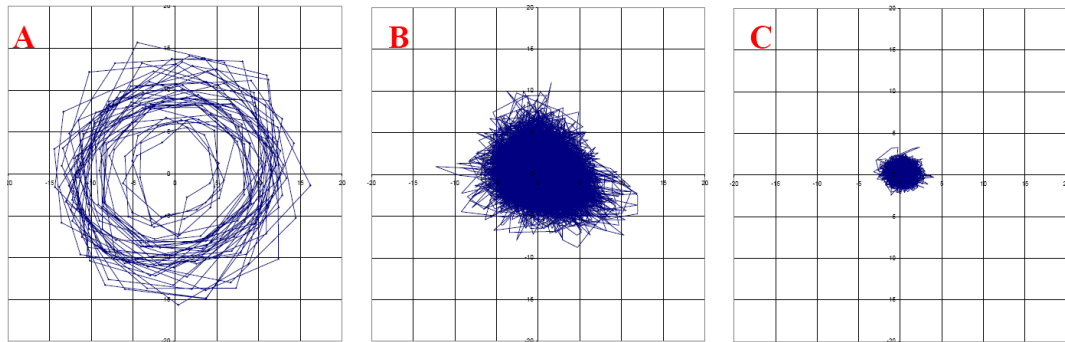
Figure 33 A, Laboratory accelerations during whirl; B, Field Acceleration during

Whirl; C, Field acceleration during No Whirl [14]

Because lateral vibration is about the center of the drill string, another analysis

method is needed to utilize the integration from the acceleration to provide us with the

53

displacement of the center. Plotting the center displacement value will give the tracers of the drill string movement.

4.3. Down-Hole Measurement Tool (Sensor Sub) Design

The measurement tool was designed by following the Sensor Configuration 3 described in the previous sections. The mechanical parts of the tool were designed by the collaboration of the author and Pushpinder Rana, and were fabricated by the machine shop in the Faculty of Engineering and Applied Science of Memorial University of Newfoundland. After the metal parts were completed, Electrical Technical Services in Faculty of Engineering and Applied Science installed the sensors on the sensor package and did the wiring for the sensor package.

The layout of the downhole measurement tool (Sensor Sub) is shown below in Figure 34.
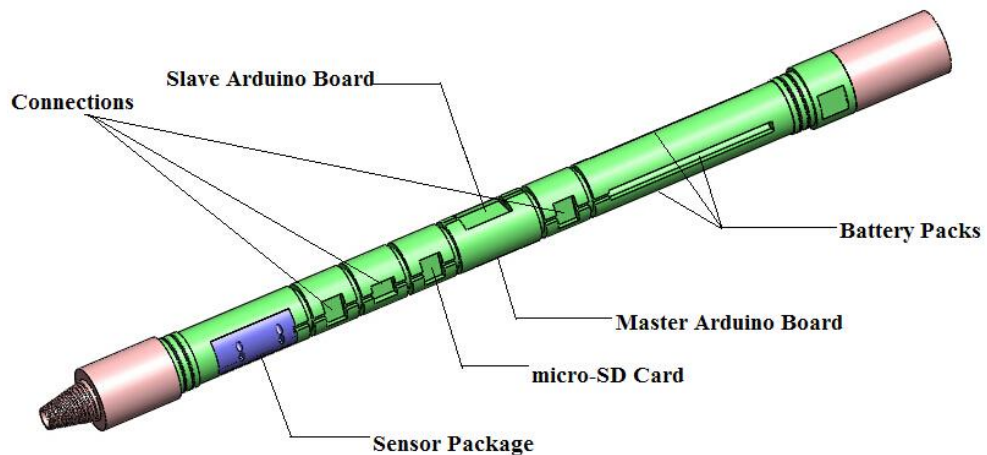
Figure 34 Layout of Downhole Measurement Tool (Sensor Sub)

The whole measurement tool comprises of one sensor package, two controllers (Arduino Boards), and three battery packs.

The two API connections are based on industrial standards, and the sensor package is located near the lower end to capture the vibrations on that end. During the tool usage operations, it can be placed near the bit to measure near bit vibration or placed in the middle section of drill string to measure the drill string vibration. The sensor package is connected to the main body with screws, and this design also reduces the torsional moment on the sensor package to avoid the potential damage to the sensors. All the sensors and controllers are covered in non-conductive silicone to keep them in place.

The power is provided by three parallel 9V battery packs. In order to avoid the batteries losing connection under severe down-hole vibration, conductive epoxy is placed between the batteries, and each pack is encapsulated in a heat shrink tube to increase the rigidity. When the batteries are put into the slot, there is foam placed around them in order to absorb the vibration during operation. Figure 35 shows an exploded view of the assembled Sensor Sub.
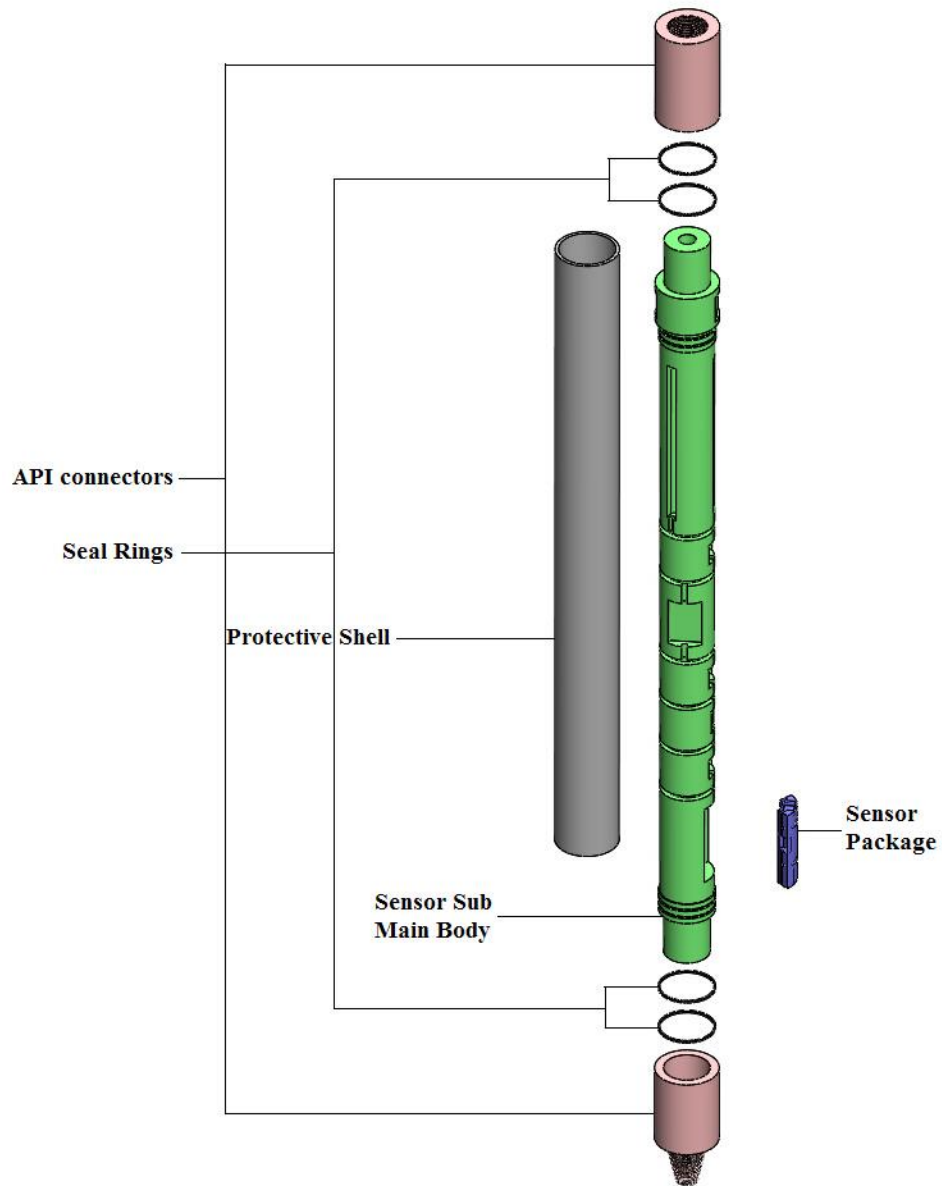
Figure 35 Exploded View of Downhole Measurement Tool (Sensor Sub)

Since the sensor package contains a magnetometer, it cannot operate near the steel. Therefore, the sensor package design utilized aluminum alloy and also the whole measurement tool. Figure 36 shows the aluminum shell that was developed to support and mount the sensors.
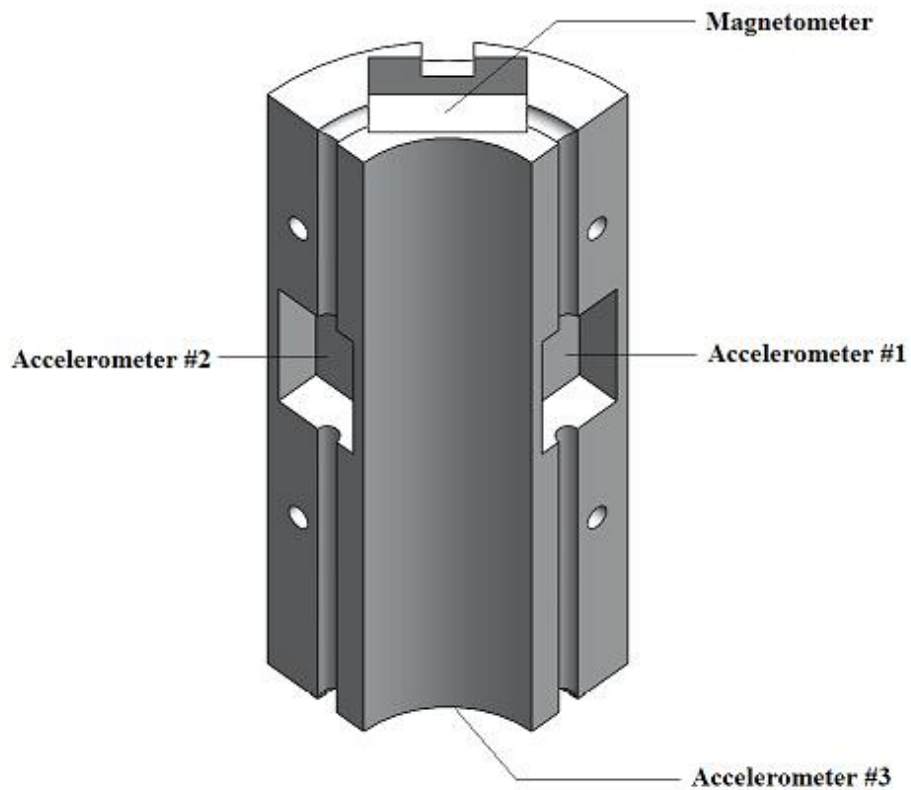
Figure 36 Sensor Package Layout

4.4. Electronic Design and Laboratory Testing

Before the measurement tool was fabricated, the electronic parts had been tested on bread boards. This test setup includes two parts: sensors are mounted on a bread board while controllers and micro-SD card are mounted on another bread board. One 9V battery pack is used to power the controllers. One set of 0.9m long wires connects these two bread boards (Figure 37). The sensors and data acquisition system used were digital with built-in anti-aliasing filters, therefore issues dealing with aliasing for signal recording were not relevant.
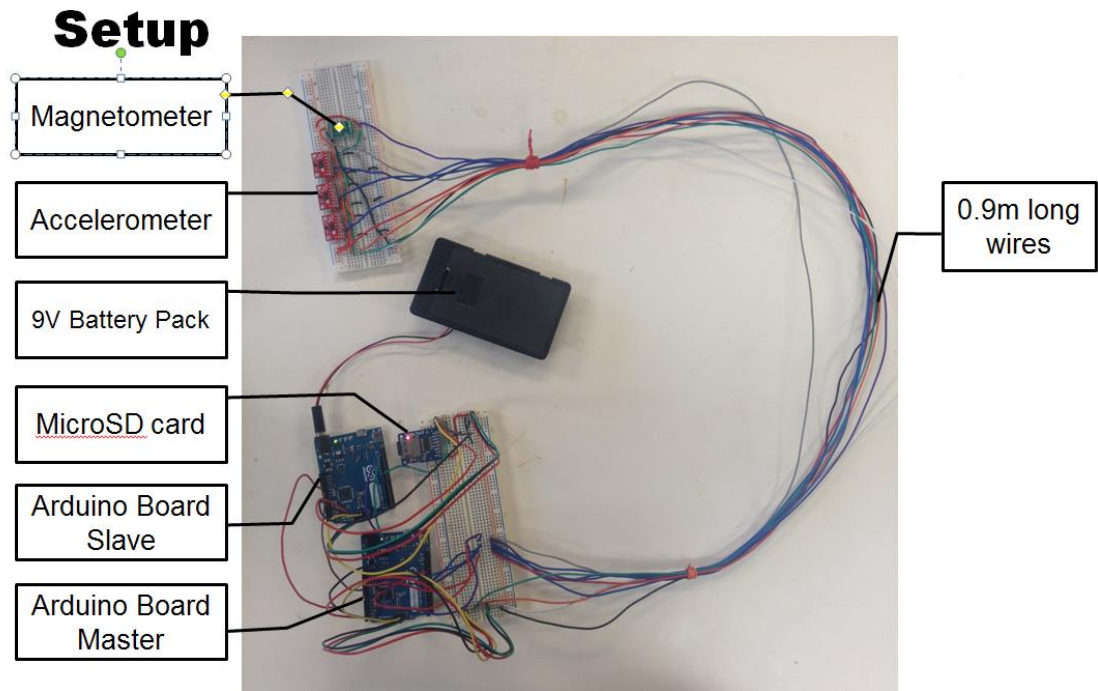
Figure 37 Setup of the Sensors

This test utilized the MTS® machine, which could move up and down or rotate at a given frequency. The sensor bread board is mounted on the arm end of the machine, and controllers are placed outside the machine. At the same time, the wire is long enough to provide the flexibility of the system so as to reduce the vibration conducted to the controllers (Figure 38).
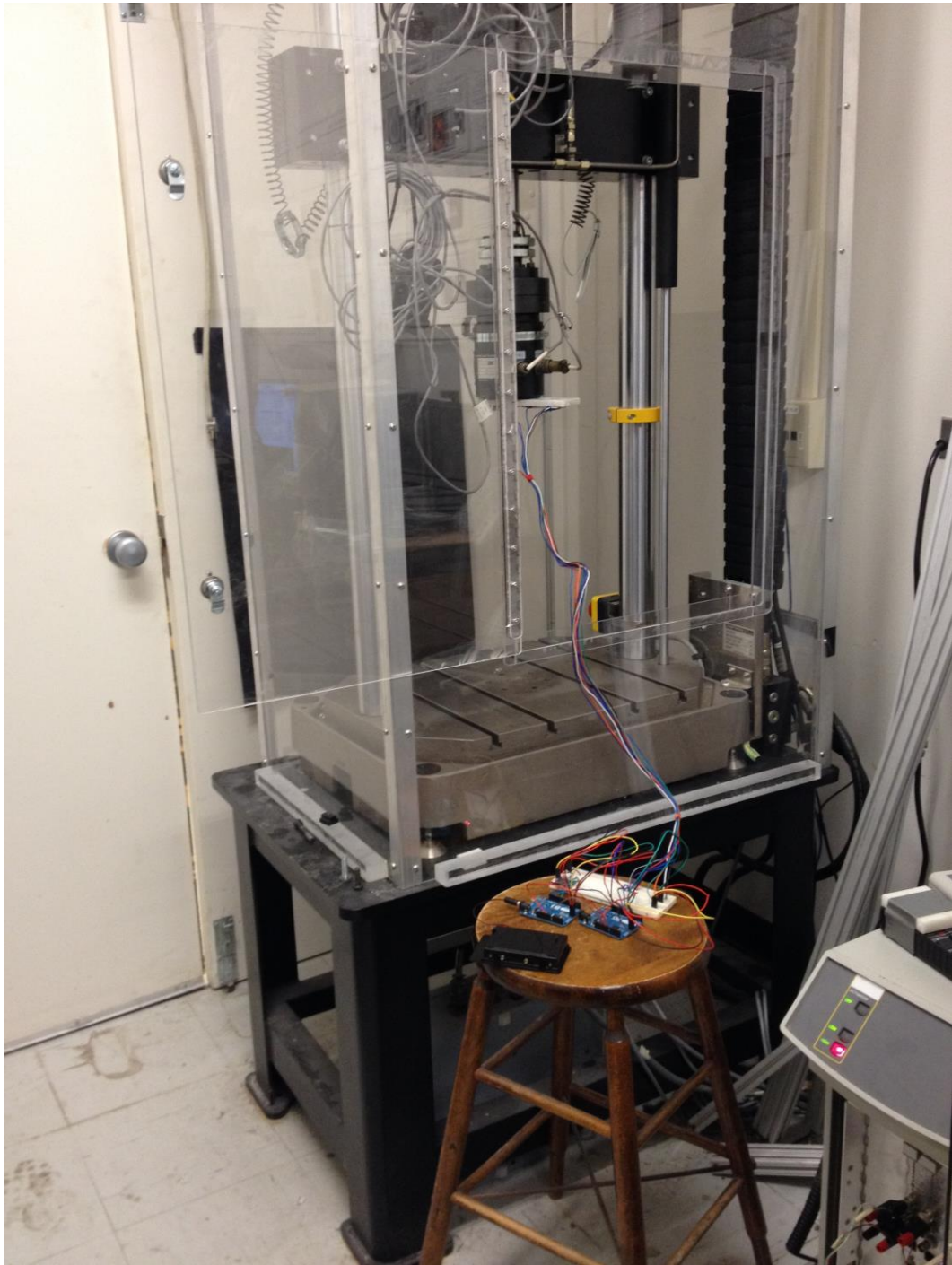
Figure 38 Setup of vertical vibration and torsional vibration testing for sensors

4.4.1. Acceleration test

The acceleration tests were conducted by setting the axial displacement of the MTS machine to move up and down at frequencies 1Hz, 2Hz, 4Hz and 10Hz, at a constant amplitude of 10 mm. The readings from these tests are given in Figure 39, Figure 40 and Figure 41.
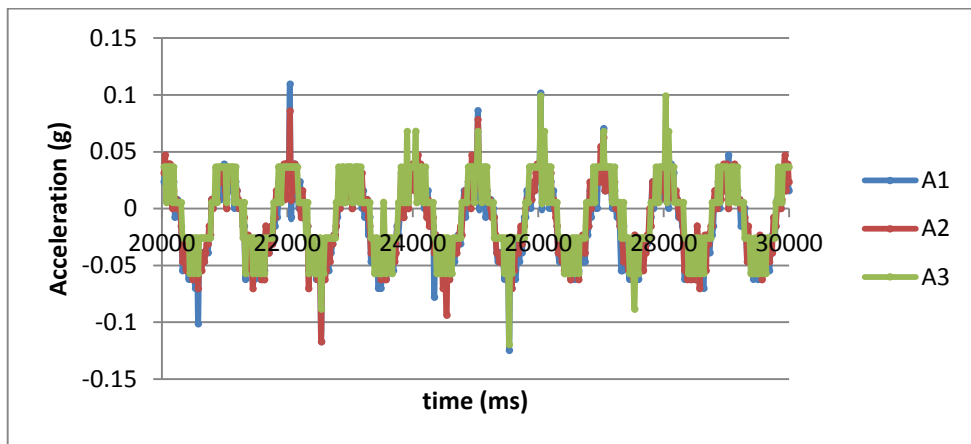
Figure 39 Sensors Reading at 1Hz
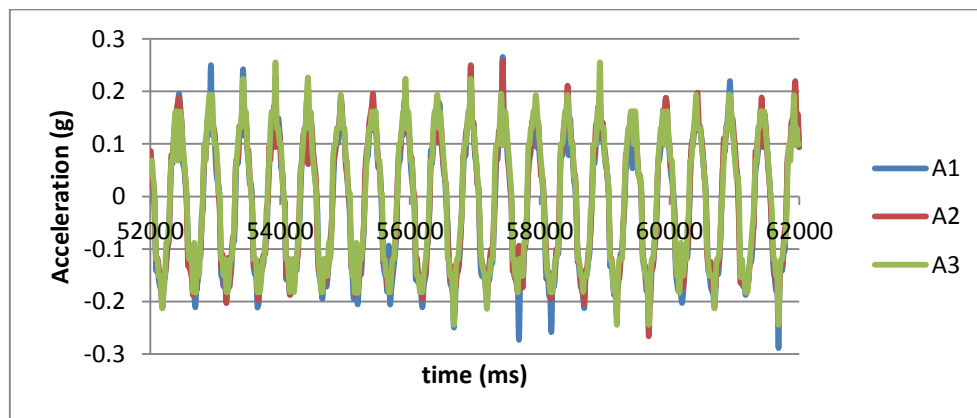
Figure 40 Sensors Reading at 2Hz
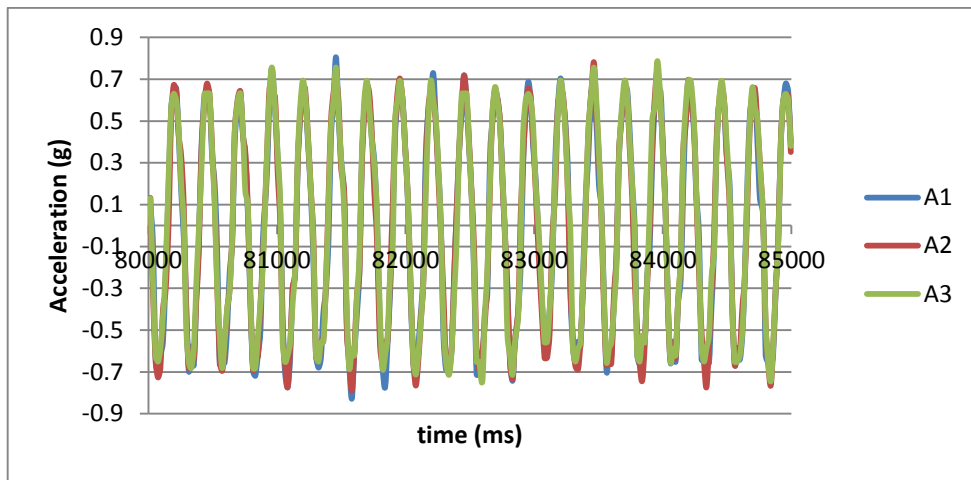
Figure 41 Sensors Reading at 4Hz

The experiment results were compared with the expected g value if the vibration is set at a given frequency and amplitude. The data contains a little noise. After filtering the accelerometer data and taking the mean value, the results of the comparison are shown in Table 2.

Table 2 Summary of acceleration test results and expected results.

	1Hz	2Hz	4Hz
expected acceleration	0.395m/s^2	1.589 m/s^2	6.317 m/s^2
expected g value	0.04 g	0.16 g	0.64 g
sensor measurement	0.04 g	0.18 g	0.65 g

The readings for 10Hz are shown in Figure 42. In 10Hz testing, the MTS machine will generate 4g acceleration. Since this experiment was conducted vertically, the acceleration due to gravity would also be recorded by the accelerometers. Because the

accelerometer A1 and A2 were set to 4g range, in this test their readings were saturated. Moreover, the vibration was severe, so it caused the whole system to vibrate at the same time. Meanwhile, the breadboard was not rigid enough, so all the readings on all accelerometers were higher than expected. For this reason, the testing result for 10Hz is not satisfactory.
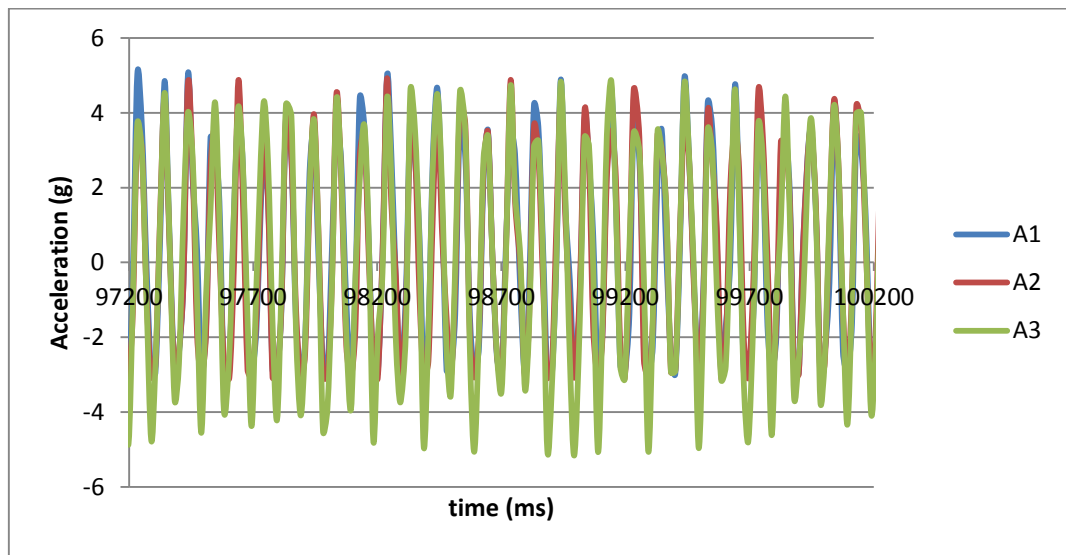
Figure 42 Sensors Reading at 10Hz

From these results we can conclude that the program is working and in low frequency all the accelerometers are working properly in low vibration frequency. And the accuracy is also satisfying. Due to the breadboard restriction, in high vibration frequency we could not get a satisfying result.

4.4.2.   Rotation Test

The rotation test was conducted to test whether the magnetometer works properly. Because the MTS machine arm is made of steel, the magnetometer readings will be

affected if it is mounted too close to the machine. A modification was done on the previous mounting (Figure 43) where a wood block was inserted between the MTS machine and the sensor bread board to increase the distance between the bread board and the machine to reduce the magnetic effect of the steel.
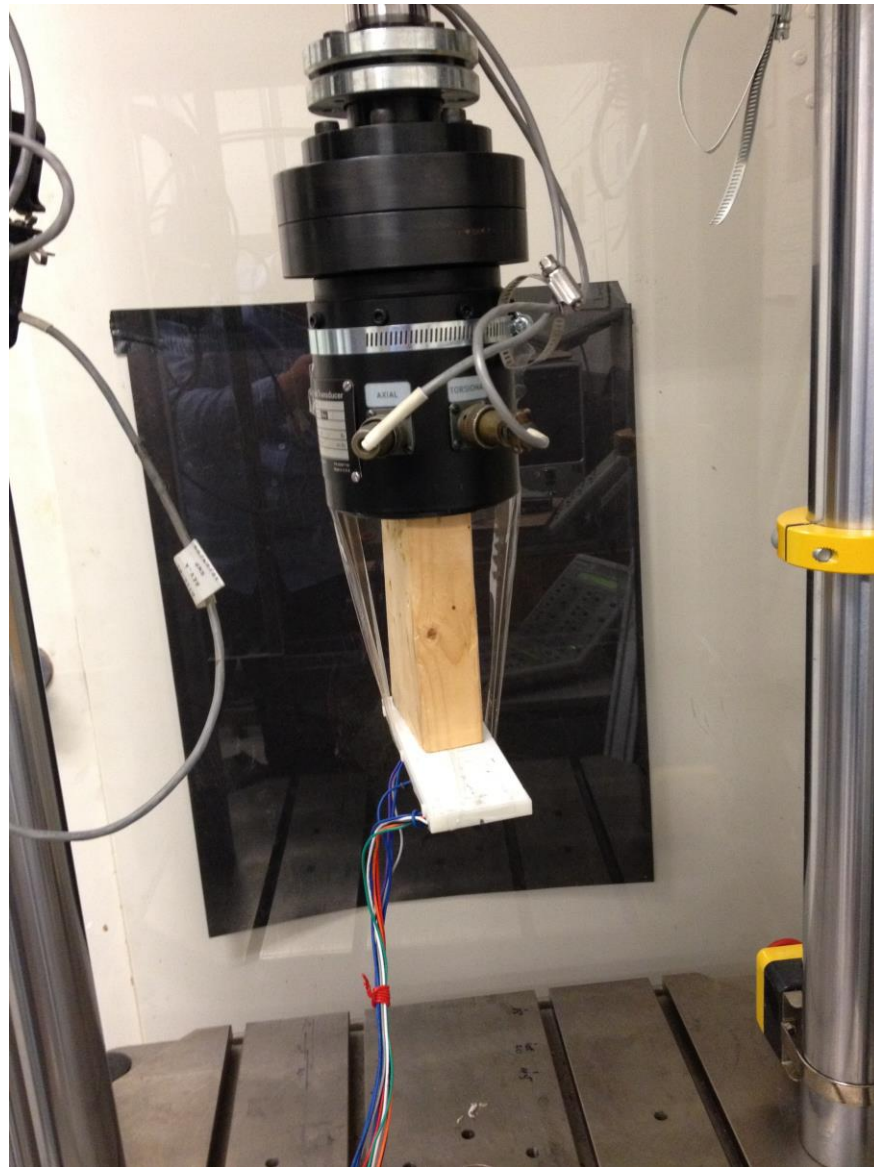
Figure 43 Magnetometer test.

One issue about this testing is that this mounting is not rigid enough, and it is also hard to locate the magnetometer at the center of the rotation. Due to these reasons, the accuracy cannot be guaranteed, and this testing can only give the magnetometer working status.
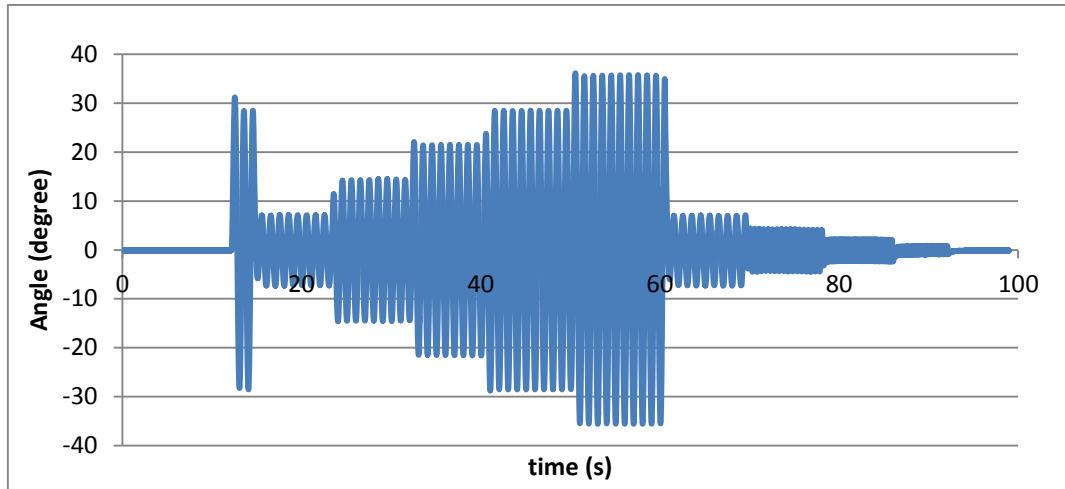
Figure 44 MTS machine Control Signal
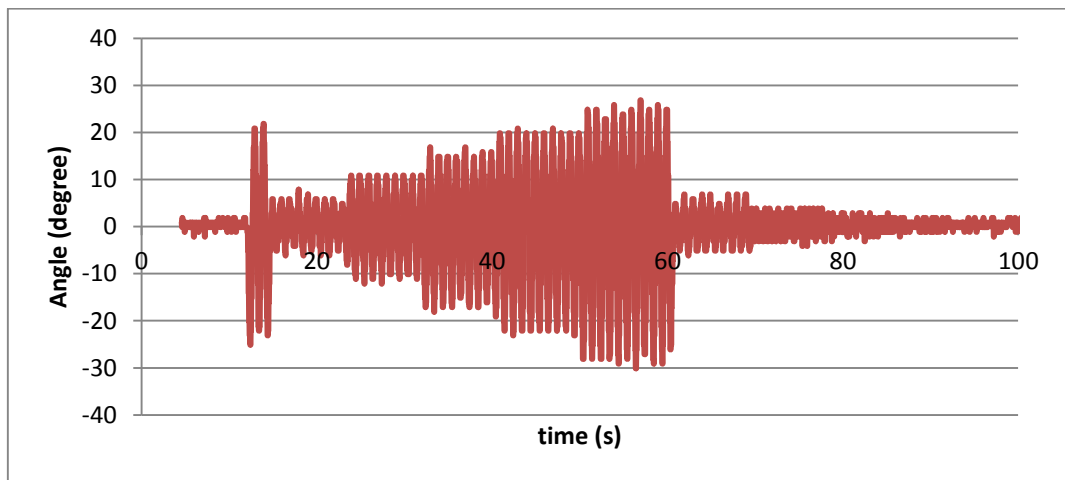
Figure 45 Magnetometer data calculated angle

4.5. Field Testing

To find out the pVARD tool performance and test the Downhole Measurement Tool functionality in field environment, field trials were conducted from September 1 to 8, 2014 at the Greenslades Construction Quarry B site (Figure 46) [30]. During field trials, drilling was conducted using both the PDC and roller cone (RC) bits with conventional rotary drilling and then repeated as needed with various configurations of the pVARD tool while penetrating the same formations under approximately equivalent WOB, scaled rotary speed, and bit hydraulic conditions. For most of these drilling runs, the pVARD tool was located directly behind the bit or Downhole Measurement Tool (Sensor Sub) in the BHA. ROP was scaled to equivalent ROP at a rotary speed of 100 rpm to account for variations in rotary speed between some intervals. Various intervals were selected for short run drilling experiments under excessive weight conditions to enhance bit wear and to induce targeted types of bit and drill string vibration. The geology in this area is gray shale, red shale and granite formation.
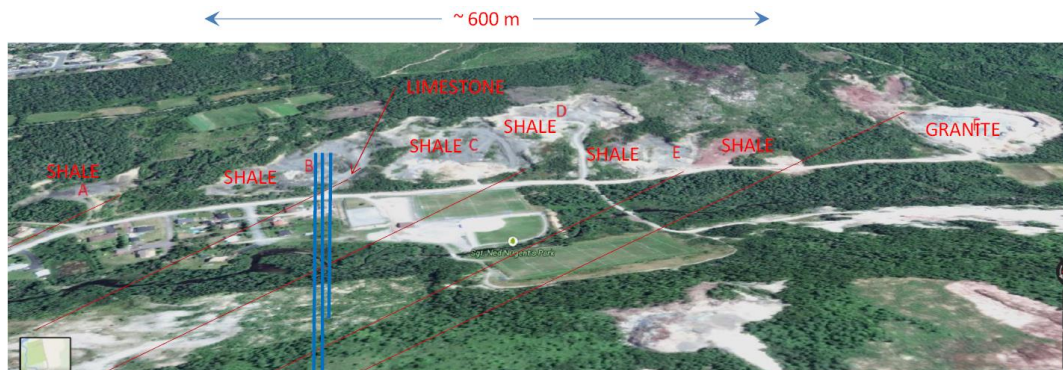
Figure 46 Aerial view of Greenslades Construction Quarry B on Red Bridge Road, Kelligrews, CBS with the approximate location of the 3 drilled wells shown in blue

Prior to tool use, the sensors were sealed in epoxy to keep them in place and to protect them from water if any leakage happened during operation. The other electronics components were encapsulated in silicone sealant to prevent the vibration damage. The tool was assembled on site as shown in Figure 47.

Figure 47 Sensors Sub before assembly

4.5.1. Field Rotation Test

Before the drilling test, the measurement tool was installed on the drill string and suspended in air with no contact with the surrounding frame. In this configuration, a free rotation test was conducted to test the magnetometer working status, as shown in Figure 48.

Figure 48 Free Rotation Test

After post processing the magnetometer data, the azimuth of the sensor pointing is shown in Figure 49, in which the 0/360 indicates the North azimuth.
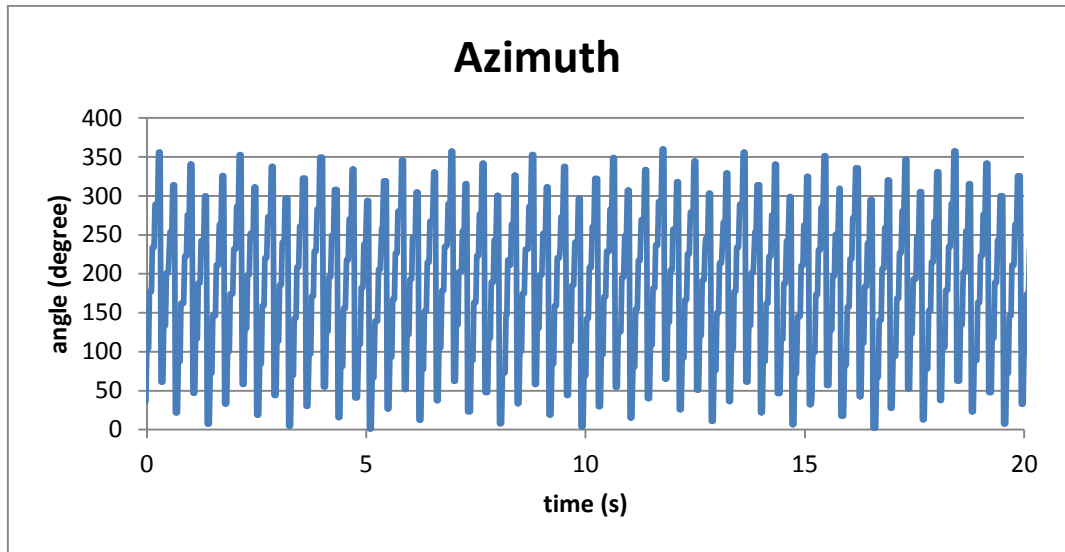
Figure 49 Azimuth of the Measurement Tool Rotation Test

Then one period was picked out to calculate the rotation speed of the drill string, as shown in Figure 50.
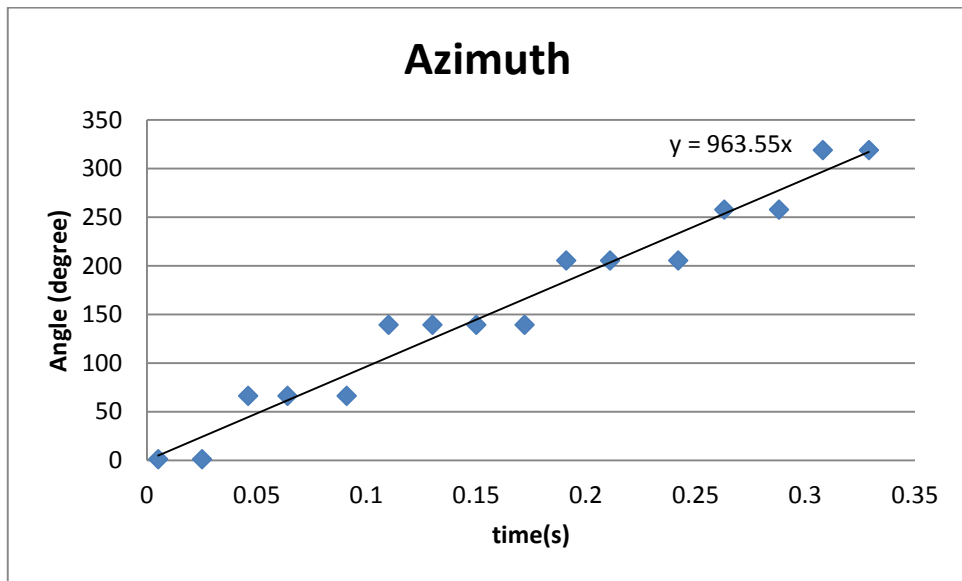
Figure 50 Example of RPM calculation

From this data, each rotation will take 360/963.55 second, which is about 161 RPM and corresponds to the maximum rotation speed of the motor with zero load and no contact with the well bore wall.

The figure below shows a time fraction of the test 2014090210, which was conducted with RC bit at WOB 28205.61 lbs, and, as the well history notes mentioned, that was a stable drilling. The figure contains about 10.5 periods and the time length was 6000ms, so each rotation took 6/10.5 second, which is 105 RPM, and was consistent with the notes on well history.
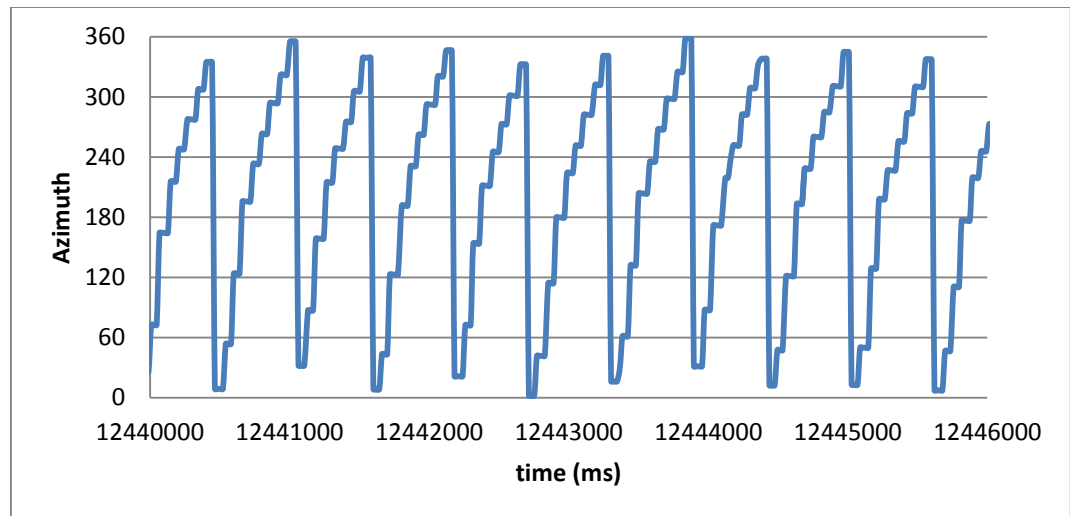
Figure 51 Rotation data Example

4.5.2. Axial Vibration

As discussed previously, the downhole measurement tool (Sensor Sub) has two accelerometers set to the 4g range and one to the 16g range. However, the recorded data is not in g, they are in 128 counts/g and 32 counts/g respectively. The axial vibration is

determined from all three accelerometers and the shock is determined from the 16g range accelerometer only.

Another conversion is the correlation between the algorithm and the actual layout in the downhole measurement. The a1x, a1y and a1z in the data are present as −A1z, A1y and −A1x in the algorithm respectively. The a2x, a2y and a2z in the data are presenting as A2z, A2x and −A2y in the algorithm, respectively.

The experiments on day 1 were conducted with a PDC bit and the experiments conducted on day 2 used a RC bit. Test numbers 2014090106 and 2014090207 have the same WOB (20739.42 lbs) and were done in the same formation (gray shale). The accelerations for these two tests were evaluated to compare the measurements recorded using both types of bits, and are summarized in Figure 52. The figure shows the PDC bit has less axial vibration than the RC bit, which indicates that the expected result corresponds to their different penetration mechanism.
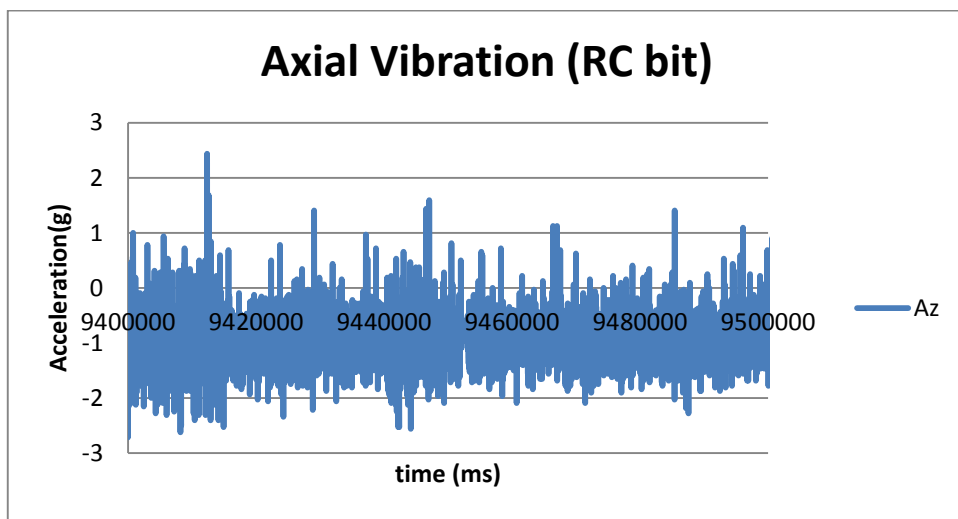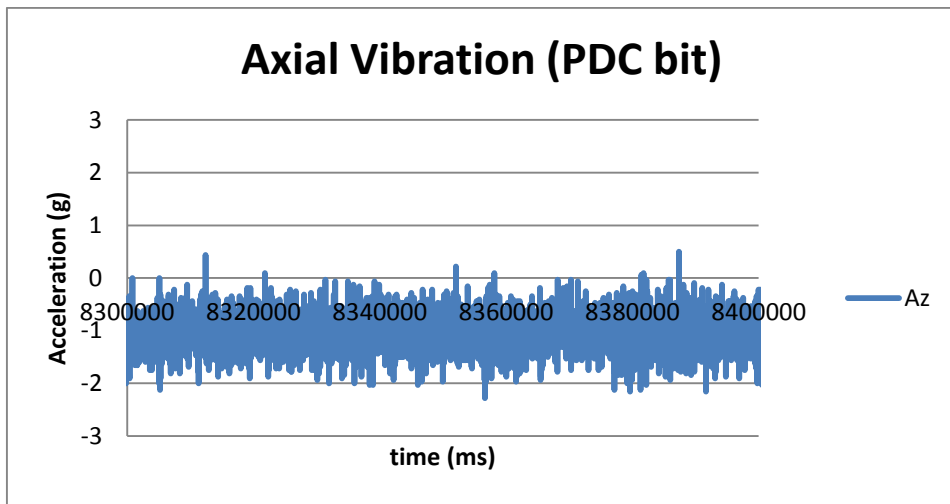
Figure 52 Axial Vibration Comparison during Drilling

The figure below shows one fraction of test 2014090204, which utilized the RC bit, and WOB was 15979.01 lbs. The peaks imply that there were shocks during the test. During this drilling test, the drilling logs indicate the formation was changed from "grey shale" to "grey and red shale", which might be the reason why the shocks happened.
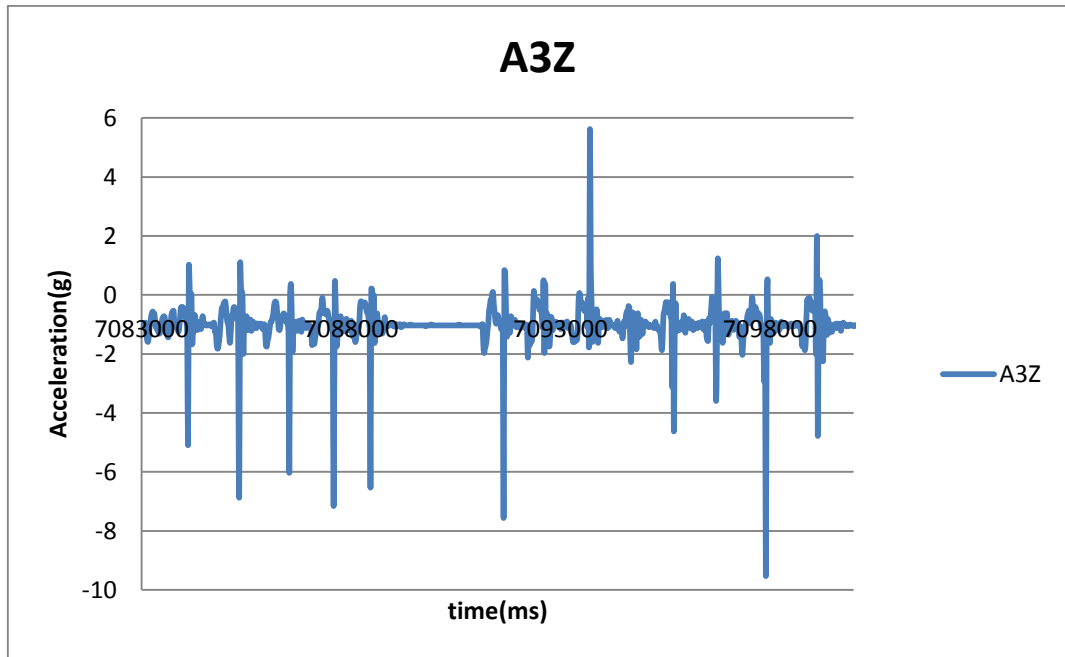
Figure 53 Shocks recorded during drilling

The value and direction of lateral vibration could also be calculated utilizing the algorithm. Figure 54 shows the results of the calculation for test 2014090201, which used RC bit under WOB 7933.01lbs and the formation was grey shale.
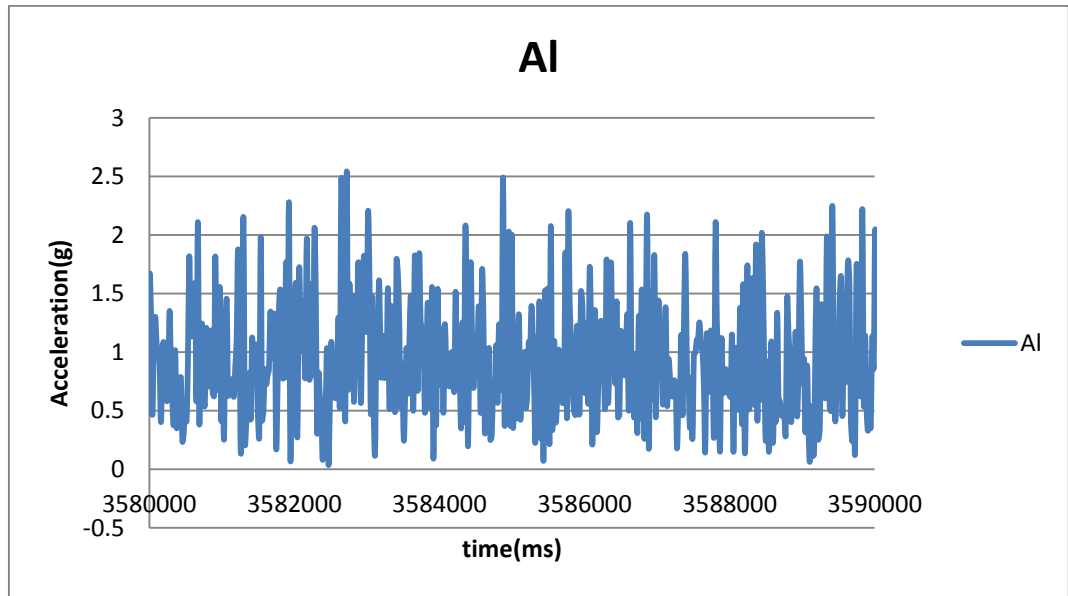
Figure 54 Lateral Vibration during Drilling
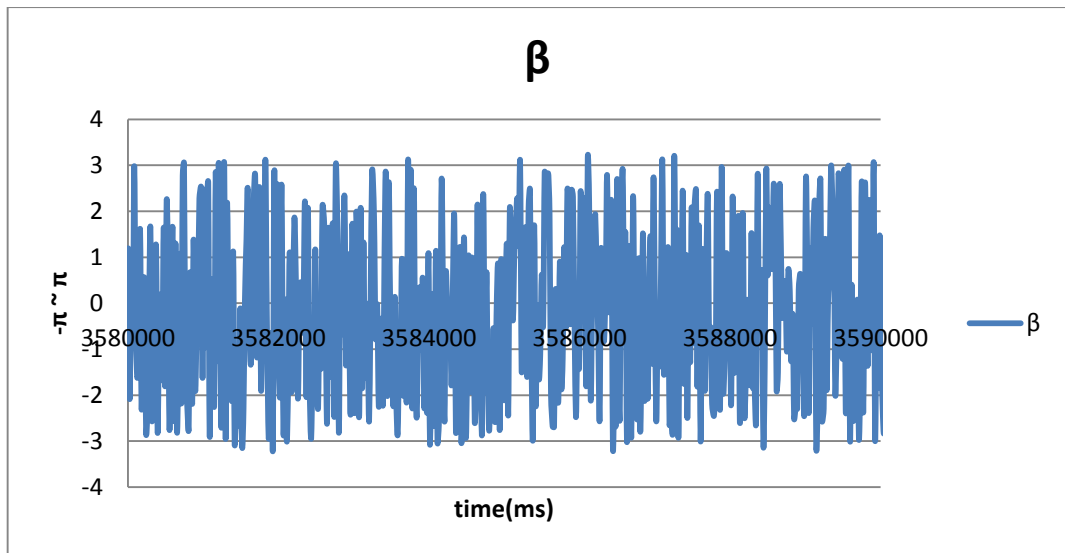
Figure 55 Lateral Vibration direction during Drilling

Figure 56 shows the lateral vibrations with PDC bit and RC bit from the same test 2014090106 and 2014090207 respectively. They are under the same WOB (20739.42 lbs) and were done in the same formation (gray shale).

From this figure we can see their performance corresponds to the characteristic of the bit. The PDC bit is much smoother than the RC bit.
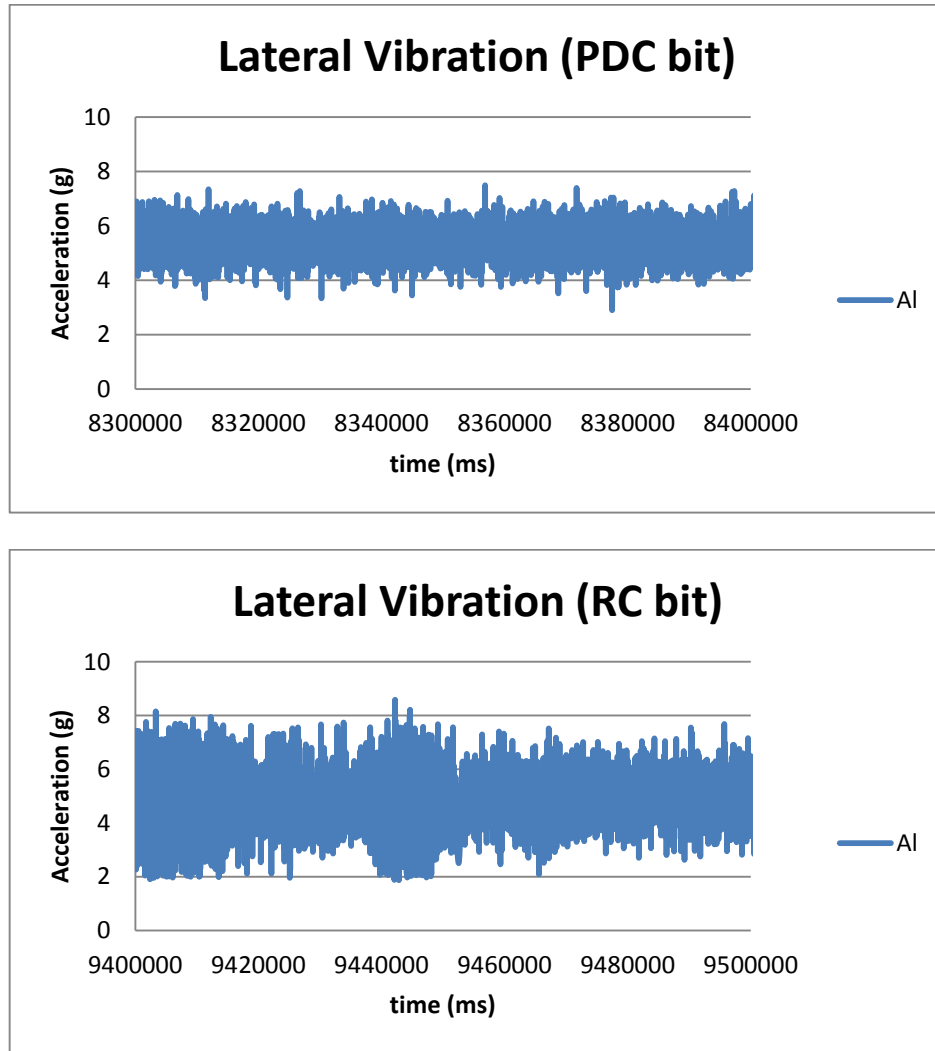
Figure 56 Lateral Vibration during Drilling

Torsion vibration during drilling can be calculated from equation 37. Figure 57 shows the torsional vibration from the same tests 2014090106 and 2014090207 respectively. They are under the same WOB (20739.42 lbs) and were done in the same formation (gray shale).

74
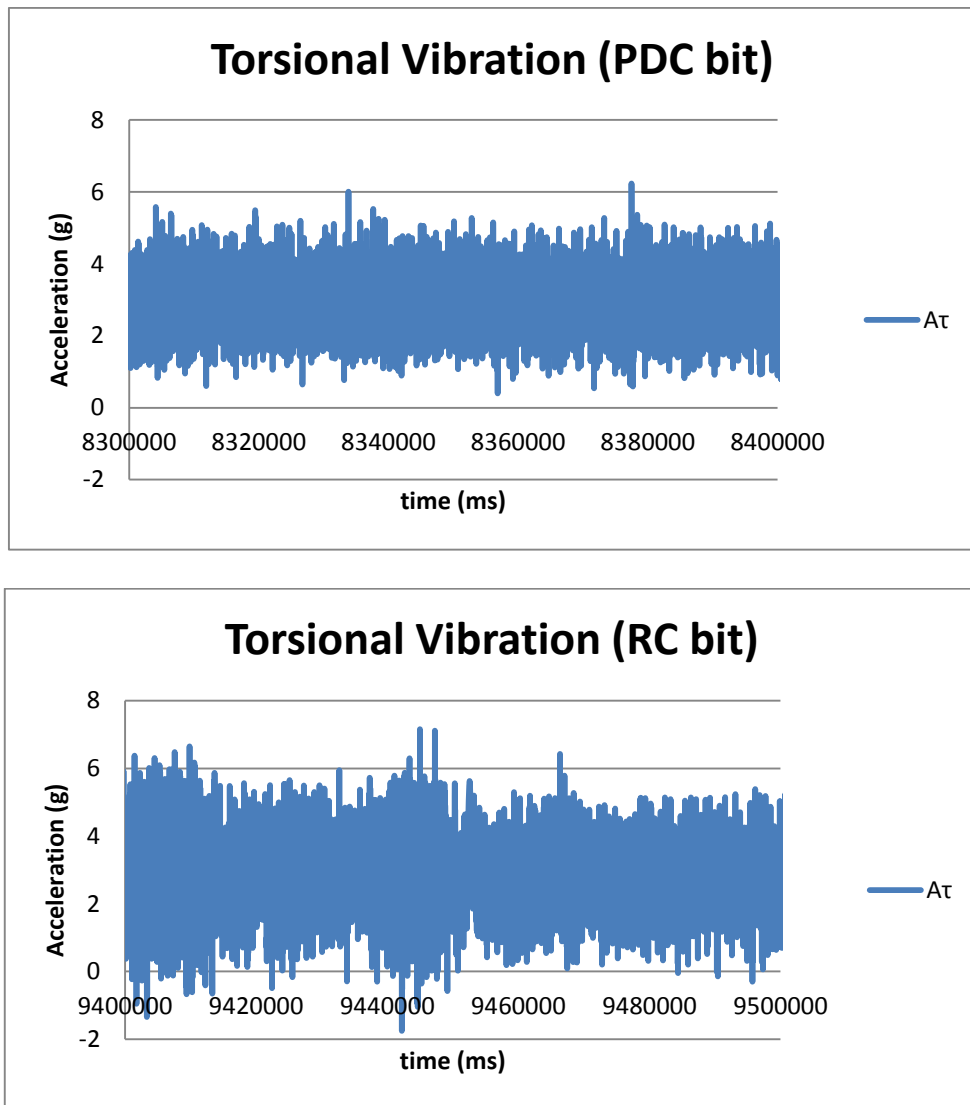
Figure 57 Torsional Vibration during Drilling

To evaluate the bit whirl, cross plots of X and Y lateral vibration were made (see Figure 33). To evaluate the lateral vibrations at the bit, lateral accelerations are an indication of high lateral motions as the bit whirls in the hole. Figure 58 shows the whirl during the test. The plot on the left is the test 2014090201 with RC bit and WOB

5807.04 lbs, and the plot on the right is the test 2014090212 with PDC bit and WOB 26546.46lbs. As expected, higher whirl is observed at higher WOB.
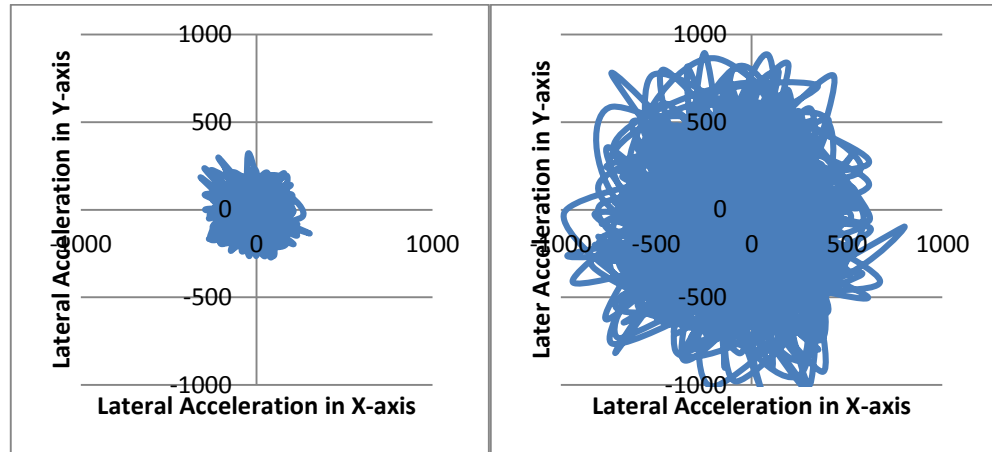
Figure 58 Analysis of whirl during test 2014090201 and 2014090212, showing low whirl (left) at low WIB and high whirl (right) at higher WOB.

4.5.3. Measurement Tool Operation Issues

In the field trial, the seal rings (see Figure 59) on one end of the Sensor Sub were damaged during the drill string dynamic testing under a very low WOB and high rotatory speed, because the drill string bounced around and contacted with the well bore, and the side force compressed the seal ring on one side, which caused the water to get in from another side. As soon as the water went in, it brought sand into the tool and damaged the seals. When we tried to open the measurement tool to retrieve the data, the tool was difficult to open. After we removed the shale from the tool, we saw lots of sand in the sealing, which scratched the aluminum shell, see Figure 59.

Figure 59 Seal was damaged after test

After this, the seal rings cannot seal the tool properly (Figure 60), so the tool was wrapped in electrical tape to prevent water interfering with the electronics for further tests. Several successful runs using the tool were made after this. However, the sealing was not sufficient and the electronics were damaged by the water and no longer worked eventually. For future work, redesign of the seals for the tool is recommended. This may be achieved by redesigning the tool so that it does not have to be disassembled to download the recorded data or to change the battery packs.

Figure 60 Wrapped measurement tool (Left) and damaged seal rings (Right)

4.6. Conclusion

In conclusion, this down-hole measurement tool (Sensor Sub) was constituted with three tri-axial accelerometers, one tri-axial magnetometer, and onboard storage, and an aluminum alloy to avoid interference from the Earth's magnetic field. Because of the special design and arrangement of the Sensor Sub, we can obtain the axial, torsional, and lateral vibration, azimuth of the tool faces, rotary speed, and even whirl data through post processing.

5.   Conclusion and Future work

From the work presented in this thesis, the SDS DAQ and control system are proved to be a success. It can record 8 different analog sensors at a high frequency simultaneously and has a friendly user interface for easy operation. The built-in emergency stop switch enhanced the laboratory safety, which is an important factor in all experimental research.

The SDS extension Mobile DAQ system extended the laboratory SDS DAQ operation. It brings a reliable DAQ system into field experiments and enhanced the experiment flexibility. The DAQ system is a well-protected system with high accuracy, high speed and high extensibility, and it can be connected to 16 different sensors at the same time and easily installed and uninstalled through quick connections.

From the field trial results, the conclusion was that the Sensor Sub worked properly, which indicated that the design and development (including sensor arrangement, system programming, and post processing algorithms) are valid. Furthermore, more tests need to be conducted in the future to ensure that the measurement tool meets the experiment requirements, especially in the field environment.

The down-hole measurement tool (Sensor Sub) is a high-speed, non-real-time data recorder prototype. It can measure down-hole axial, torsional, lateral vibration, stick-slip, well inclination, and back calculate whirl. This will provide the Advanced Drilling Laboratory with field data to help improve the simulation experiments.

In addition, SDS and Mobile DAQ are finished products; the future work on these two systems will be regular maintenance and calibration. Modification could be done easily based on the experimental requirements.

The down-hole measurement tool (Sensor Sub) is a non-real-time data recorder first generation prototype. The installation and wiring could bring some error or noise into this system. In the future, a new design on mechanical components would be recommended so as to provide better sealing and make the next generation prototype on a single PCB board, which could enhance the performance and the accuracy of the system to some extent. Moreover, the casing of the tool could be modified to have an easy access to the data and the battery without having to pull the tool apart.

Because this measurement tool is a non-real-time data recorder, all the data we obtained need a post processing to get complete motion data. In the future work, if the controller could be more powerful, we might be able to calculate all the data in real time and this measurement tool could work with a mud pulse telemetry tool or wire-line to develop a real-time down-hole measurement system. Besides, the experiment results proved that the algorithms are accurate, which implies that the data collected from the field trial can be used for further research.

Reference

1 Offshore Rig Day Rates. (2014, June). (Dice Holdings, Inc.) Retrieved from Rigzone: https://www.rigzone.com/data/dayrates/

2 Li, H., Butt, S., Munaswamy, K., & Arvani, F. (2010). Experimental Investigation of Impact of Bit Vibration on Rotary Drilling Penetration Rate. St.John's: ARMA.

3 Babatunde, Y., Butt, S., Molgaard, J., & Arvani, F. (2011). Investigation of the Effects of Vibration Frequency on Rotary Drilling Penetration Rate Using Diamond Drag Bit. St. John's: ARMA.

4 Pronin, O. (2012). Pulse-Cavitation Vibrating Drilling Prototype Development and Evaluation. St.John's: Memorial University of Newfoundland

5 Babapour, S. & Butt, S. (2014). Investigation of Enhancing Drill cuttings Cleaning and Penetration Rate Using Cavitating Pressure Pulses. St.John's. ARMA.

6 Gharibiyamchi, Y. (2014). Evaluation and Characterization of Hydraulic Pulsing Drilling Tools and Potential Impacts on Penetration Rate. St.John's: Memorial University of Newfoundland

7 Rowsell, P.J. and Waller, M. D. (11-14 March, 1991). Intelligent Control of Drilling Systems. Amsterdam: SPE/IADC.

8 Hu, Q., & Liu, Q. (5-7 December 2006). Intelligent Drilling: A Prospective Technology of Tomorrow. Beijing: SPE.

9 Arnaout, A., Fruhwirth, R., Esmael, B., & Thonhauser, G. (2012). Intelligent Real-time Drilling Operations Classification Using Trend Analysis of Drilling Rig Sensors Data. Kuwait City: SPE.

10 Decker, D., & Burgess, T. R. (1993). At the Bit Technology Improves Horizontal Drilling Performance. New Drilling Technology.

11 Pastusek, P., Sullivan, E., & Harris, T. (2007). Development and Utilization of a Bit-Based Data-Acquisition System in Hard-Rock PDC Applications. Amsterdam, Netherlands: SPE/IADC.

12 Zannoni, S. A., Cheatham, C. A., Chen, C.-K. D., & Golla, C. A. (1993). Development and Field Testing of a New Downhole MWD Drillstring Dynamics Sensor. Houston,Texas: SPE.

13 Finger, J. T., Mansure, A. J., Knudsen, S. D., & Jacobson, R. D. (2003). Development of a System for Diagnostic-While-Drilling (DWD). Amsterdam, Netherlands: SPE/IADC.

14 Mansure, A. J., Finger, J. T., Knudsen, S. D., & Wise, J. L. (2003). Data Interpretation of Diagnostics-While-Drilling. Denver, Colorado: SPE.

15 Cobern, M. E., & Wassell, M. E. (2004). Drilling Vibration Monitoring & Control System. Cromwell,CT.

16 Pastusek, P., Sullivan, E., & Harris, T. (2007). Development and Utilization of a Bit-Based Data-Acquisition System in Hard-Rock PDC Applications. Amsterdam, Netherlands: SPE/IADC.

17 Sullivan, E. C., & Pastusek, P. E. (2010, April 22). Patent No. US 2010/0097890 A1. United States.

18 Abtahi, A., Butt, S., Molgaard, J. & Arvani, F. (2011). Wear Analysis and Optimization on Impregnated Diamond Bits in Vibration Assisted Rotary Drilling (VARD). San Francisco: ARMA

19 Honeywell. (2008, May). Model 3173 Tension/Compression Pancake Load Cell. Golden Valley, MN, USA.

20 Endress+Hauser. Cerabar T PMP131. Weil am Rhein: Endress+Hauser GmbH+Co.KG Instruments International

21 GE Measurement & Control Solutions. UNIK 5000 Pressure Sensing Platform. s.l.: GE Measurement & Control Solutions.

22 Sakae. MODEL 30LP.

23 Crossbow Technology. Accelerometers, General purpose, LP series. San Jose: s.n. 6020-0001-01.

24 Pacific Scientific-OECO. Model CLN-50/100. Milwaukie: Pacific Scientific-OECO.

25 Omega. User's guide Series FTB-1400 Turbine Flow Meter. Laval: Omega.

26 National Instruments Corporation. DAQ E Series (E Series User Manual). s.l. : National Instruments Corporation, 2007.

27 Khorshidian, H., Mozaffari, M. and Butt, S. D. (2012). The Role of Natural Vibrations in Penetration Mechanism of a Single PDC Cutter. St. John's: ARMA

28 Wassell E. Mark. Vibration Monitoring System for Drillstring. 5226332 U.S., July 13, 1993.

29 Ozyagcilar, Talat. Implementing a Tilt-Compensated eCompass using Accelerometer and Magnetometer Sensors. s.l. : Freescale Semiconductor Inc., 2012. AN4248

30. Butt, S. (2014). Unpublished Report for Husky Energy, Suncor Energy and Noble Drilling Canada.

Appendices

A-1.   Load cell calibration

The steps of calibration for pressure transducer are as follows:

1)   Connect the circuit, follow the circuit diagram

2)   Use a multi-meter to make sure the circuit is correct

3)   The calibration sheet for the load cell and amplifier are available from factory.

The data input needs to be converted from voltage into load. The calibration sheet for the load cell and the amplifier are in Figure 61 and   Figure 62.

Honeywell
load cell

2080 Arlingate Lane
Columbus, Ohio 43220 U.S.A.
Phone 614-850-5000
Toll free 800-848-6564
Fax 614-850-1111
www.honeywell.com/sensotec
sensotec.service@honeywell.com

CERTIFICATE OF CALIBRATION
Product Identification

Product Type:	LOAD	Part No.:	3173-2K
Model:	3173-2K	Order Code:	3173-2K,1AD,2U,6AB,15C
Serial No.*:	1309064A	Instrument Serial No.:	N/A

* A letter at the end of the serial number indicates the associated bridge

Product Specifications

Capacity:	2000lbs	Excitation:	10.0 Vdc
Calibrated At:	2.00Klbs	Amplifier Output:	N/A
Direction / Type:	Compression	Electrical Leakage:	∞ MegΩ

Calibration Data

Shunt Cal Factor:	-1.4568 mV/V	Input Resistance:	701 Ω	Calibration Factor:	-2.2033mV/V
Shunt Cal Resistor:	120000 Ω	Output Resistance:	701 Ω	Calibration Date:	06/24/2010

Calibration Procedure: 072-LC75-10, Rev -, Date 02/19/2008

Wiring Code

UNAMP,4-COND,5-COND,6-COND,4-PIN,5-PIN,6-PIN

4-PIN		5-PIN		6-PIN	
PIN	FUNCTION	PIN	FUNCTION	PIN	FUNCTION
A	(+)EXC.	A	(+)EXC.	A	(+)EXC
B	(+)SIG.	B	(+)SIG.	B	(+)SIG.
C	(-)SIG.	C	(-)SIG.	C	(-)SIG.
D	(-)EXC.	D	(-)EXC./	D	(-)EXC.
			TEDS GND	E	TEDS GND
		E	TEDS DATA	F	TEDS DATA

* USE TEDS CONNECTIONS WHEN REQUIRED
001-LWR-100

Calibration Data

% Capacity	Load [Klbs]	Raw (mV/V)	Normalized (mV/V)
0	0.00	-0.0169	0.0000
25	0.50	-0.5677	-0.5508
50	1.00	-1.1186	-1.1017
75	1.50	-1.6692	-1.6523
100	2.00	-2.2195	-2.2026
75	1.50	-1.6700	-1.6531
50	1.00	-1.1187	-1.1018
25	0.50	-0.5676	-0.5507
0	0.00	-0.0163	0.0006

Environmental Data

Temperature: 75 °F	Humidity: 58 %RH	Pressure: 14.28 psiA

Figure 61 Calibration sheet for Load Cell

DATAFORTH CORPORATION
3331 E. Hemisphere Loop
Tucson, AZ 85706 USA

Phone: (520) 741-1404
Fax: (520) 741-0762
email: info@dataforth.com

TEST DATA SHEET

Date: 01-12-2012
Model: DSCA38-12C
SN: 64661-5

ACCURACY TEST

Vin (mV)	Calculated Output (mA)	Measured Output (mA)*	Error (%)	Status
-20.005	+3.998	+3.994	-0.027	PASS
-10.007	+7.997	+7.995	-0.015	PASS
+0.002	+12.001	+12.002	+0.007	PASS
+9.988	+15.995	+15.996	+0.005	PASS
+19.997	+19.999	+20.001	+0.013	PASS

FINAL TEST RESULTS

Parameter	Measured Value*	Specification	Status
Supply Current	40.0 mA	< 60 mA	PASS
Supply Curr. w/ EXC Load	64.0 mA	< 100 mA	PASS
Excitation Voltage	9.998 V	10+/-.003 V	PASS
Exc. Load Regulation	-4 ppm/mA	+/- 11 ppm/mA	PASS
Output Reg. w/ EXC Load	0.00 %	+/- .05 %	PASS
Excitation Current Limit	54 mA	< 65 mA	PASS
Linearity	0.010 %	+/- .02 %	PASS
Accuracy	-0.027 %	+/- .05 %	PASS
Power Supply Sensitivity	0.0001 %/%	+/- .0006 %/%	PASS
Frequency Response	28.4 dB	28+/- 5 dB	PASS
Output Noise	1.0 uArms	<= 5 uArms	PASS
Chg. in Iout w/ Max Load	0.034 %	+/- .3 %	PASS
240VAC Withstand			PASS
Hi-Pot			PASS

Check List

Tested by: _____Bn⌐____   QC: _____   QC
                                                           13

It is hereby certified that the above product is in conformance with
all requirements to the extent specified. This product is not
authorized or warranted for use in life support devices and/or systems.

* NIST traceable calibration certificates support Measured Value data.
  Calibration services are available through ANSI/NCSL Z540-1 and
  ISO Guide 25 Certified Metrology Labs.

Figure 62 Calibration sheet for Amplifier

A-2.   Pressure transducer calibration 1

The steps of calibration for the pressure transducer are as follows:

1)   Connect the circuit, follow the circuit diagram

2)   Use a multimeter to make sure the circuit is correct

3)   The pressure transducer is calibrated in the factory, 0-5V input was used and

the calibration sheet is shown in Figure 63.

OMEGADYNE   INC.

PRESSURE TRANSDUCER
FINAL CALIBRATION

0.00 -   30.00 PSIG
Excitation   28.000 Vdc

Job: TN1663
Model: PX319-030GI
Date: 3/7/2011
Calibrated: 0.00 -   30.00 PSIG

Serial: 1130101036
Tested By: JP
Temperature Range: 4 to 185 F.
Specfile: PX319-I--15--50G--3

Pressure   Unit Data
PSIG   mA
---------- ------------
   0.00   4.013
  15.00   12.027
  30.00   20.010
  15.00   12.029
   0.00   4.015

Balance   4.013   mA
Sensitivity   15.997   mA

ELECTRICAL LEAKAGE: PASS
PRESSURE CONNECTION/FITTING: 1/4-18 NPT Male
ELECTRICAL WIRING/CONNECTOR: Pin 1 = +EXC
                             Pin 2 = -EXC

This Calibration was performed using Instruments and Standards that are
traceable to the United States National Institute of Standards Technology.
S/N   Description   Range   Reference   Cal Cert
0495/91-4   AUTO 50/500 PSI DRUC 0 - 500 PSIG   C-2508   C-2508
US37026070   AT34970 DMM   Unit Under Test   C-2492   C-2492

Q.A. Representative : John Piendl   Date: 3/7/2011
This transducer is tested to & meets published specifications. After final
calibration our products are stored in a controlled stock room & considered in
bonded storage. Depending on environment & severity of use factory calibration
is recommended every one to three years after initial service installation date.

Omegadyne, Inc., 149 Stelzer Court, Sunbury, OH 43074   (740) 965-9340
http://www.omegadyne.com   email: info@omegadyne.com   (800) USA-DYNE

Figure 63 Calibration sheet for Pressure Transducer1500psi

A-3.   Pressure transducer calibration 2

The steps of calibration for the pressure transducer are as follows:

1) Connect the circuit, follow the circuit diagram

2) Use a multimeter to make sure the circuit is correct

3) The calibration sheet for the pressure transducer came from the factory, use the

calibration data to convert the 0-5V input to pressure. The calibration sheet is in Figure

64.
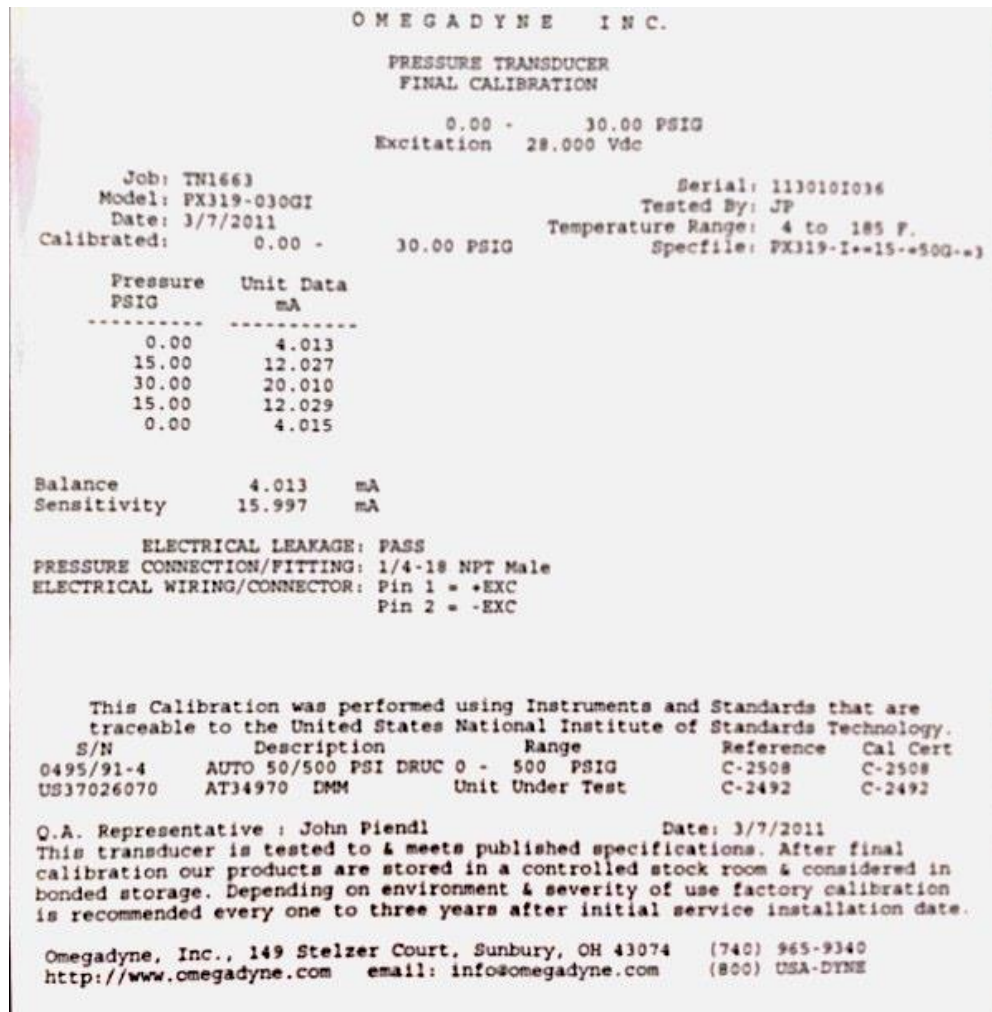
Figure 64 Calibration sheet for Pressure Transducer 1000psi

A-4.   Pressure transducer calibration 2

The steps of calibration for the LPT are as follows:

1) Connect the circuit, follow the circuit diagram

2) Use a multimeter to make sure the circuit is correct

3) Let the LPT be fully extended, and then record the output voltage V1; let the LPT stroke fully pull back, and record the output voltage V2; then measure the effective length L. Make the fully extended stroke position 0.

4) The conversion formula is for position P and input voltage v

$$P = \frac{V2 - V1}{L} v$$

A-5.   Rotary encoder calibration

The steps of calibration for the rotary encoder are as follows:

1) Connect the circuit, follow the circuit diagram

2) Use a multimeter to make sure the circuit is correct

3) Because only one signal is used to record the rotary speed, the number of pulses should be converted to revolutions. Through the test, the rotary encoder will generate a 1000-pulse signal, and by using this data and the clock time (s) built inside the LabVIEW software, the rotary speed can be calculated

4) The conversion formula to get rotary speed N from pulse number n is

$$N = \frac{n}{1000 * t} * 60$$

A-6.   Accelerometer calibration

The steps of calibration for the accelerometer are as follows:

1) Connect the circuit, following the circuit diagram

2) Use a multimeter to make sure the circuit is correct

3) Because only one signal is used to record the rotary speed, the number of pulses should be converted to revolutions. Through the test, the rotary encoder will generate a 1000-pulse signal, and by using this data and the clock time (s) built inside the LabVIEW software, the rotary speed can be calculated

4) The conversion formula to get rotary speed N from pulse number n is

$$N = \frac{n}{1000 * t} * 60$$

A-7.   Hall Effect Sensor Calibration

The steps of calibration for the Hall Effect sensor are as follows:

1)   Connect the circuit, follow the circuit diagram

2)   Use a multimeter to make sure the circuit is correct

3)   The circuit is powered by $\pm15V$ DC and the nominal analog output of the sensor is 50mA, which is indicated as the nominal current 50A rms.

A-8.   Flow meter calibration

The steps of calibration for the flow meter are as follows:

1) Connect the circuit, follow the circuit diagram

2) Use a multimeter to make sure the circuit is correct

3) From the sensor specification, each gallon that passes through the flow meter will generate 870 pulse signals.

4) The conversion formula to get flow amount M from pulse number n is

$$M = n/870$$

1) The flow rate R through the recording time t (in system can set every 10s) is

$$R = M/t$$

A-9. SDS System Computer Enclosure
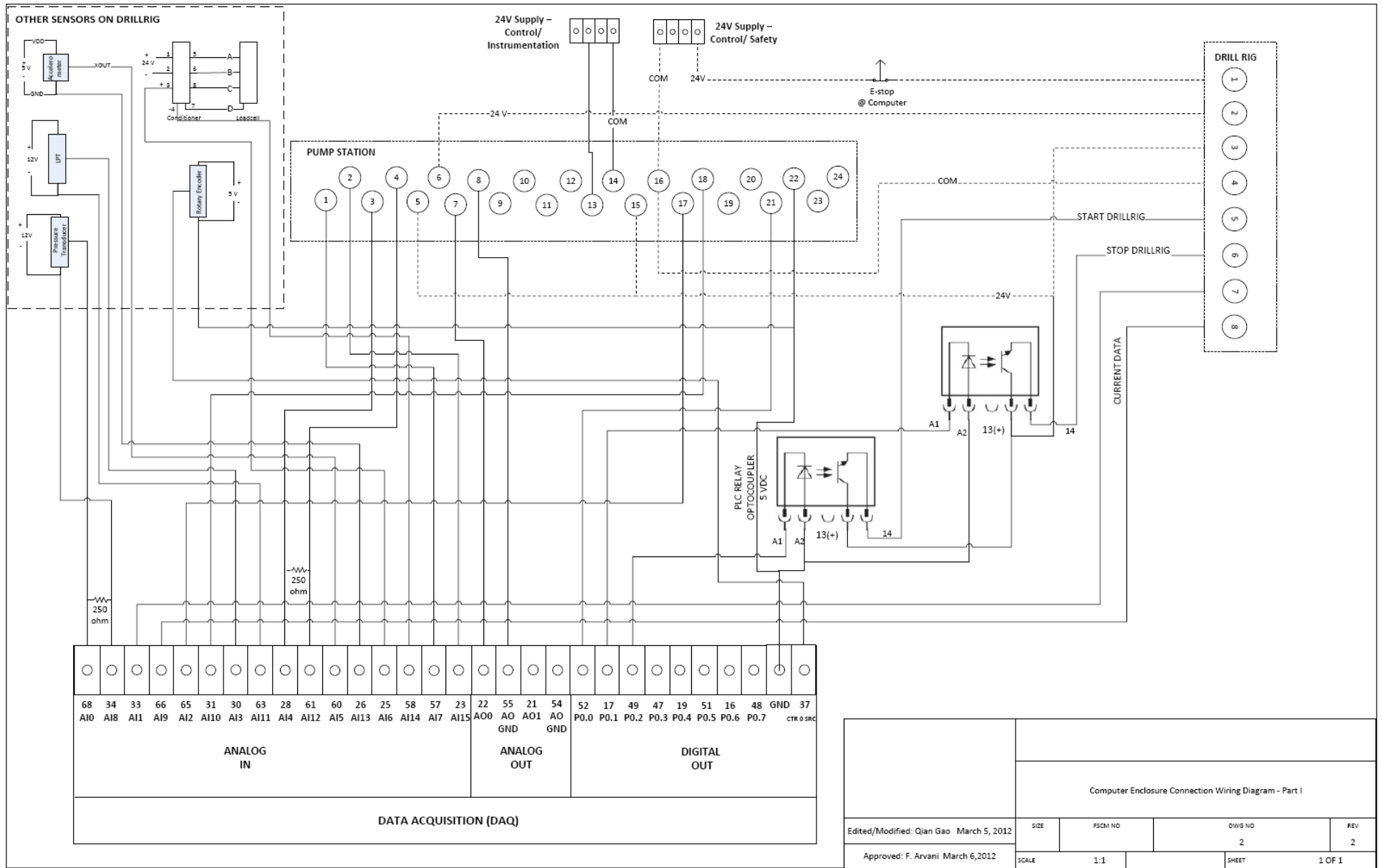
Computer Enclosure Connection Wiring Diagram - Part I

Edited/Modified: Qian Gao March 5, 2012

Approved: F. Arvani March 6,2012

A-10. SDS System Connection Diagram

Drill Rig Circuit Schematic

	Terminal Legend	
① ②	E-Stop Switch	
③ 24V ④ COM	Main Power Supply	
⑤	Remote Start Drillrig	
⑥	Remote Stop Drillrig	
⑦ ⑧	Motor Current Sensor Output	
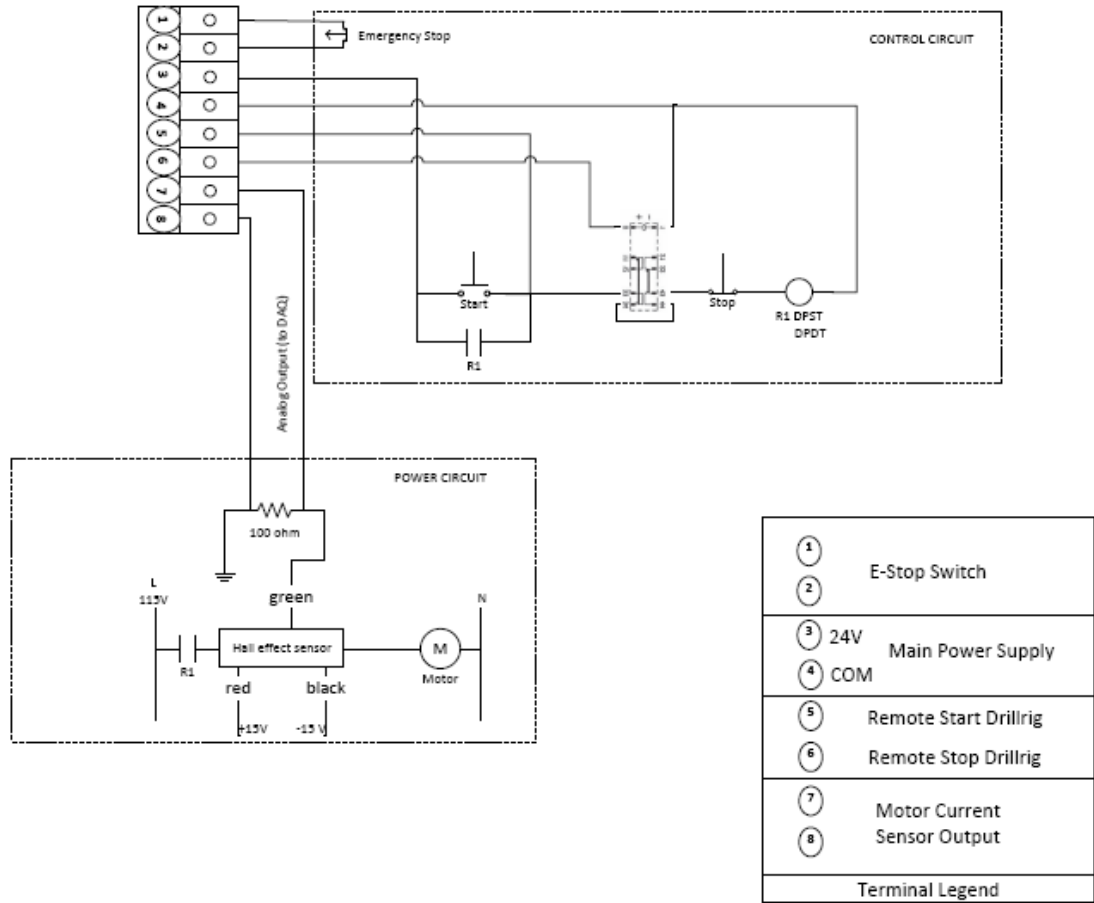
REVISED						
4/16/2012						
			Drill Rig Circuit Schematic			
Edited/Modified: Qian Gao March 5, 2012	SIZE	FSCM NO		DWG NO 1		REV 3
Approved: F. Arvani March 6,2012	SCALE	1:1		SHEET	1 OF 1	

Sheet.251

4-20mA: Remote speed Control

RELAY SAFETY 4PST 6A 24V

AO: 0-10VDC: Power(KW)

Remote Start

PLC RELAY OPTOCOUPLER 5VDC

24V

COM

| 1 | 2 | 5 | 6 | 25 | 4 | 11 | 13A | 13B | 13C | 13D | 14 | 30 | 2 | TXA | TXB | 16 | 17 |

Speed Dial 10K

Tank Empty: Orange lenz

Pumping:: Green lenz

Fault: Red lenz

COM 24V

LT

Refer to table A for coding
Yel
Pur
Brn

Reserved

PT

E-stop @ Pump

24V

24V

2R 1R

PI (Diag. B)

8R
7R
4/6 R

1P 6P

400 mA
24V

COM

24V Supply

FT

4-20mA loop

4-20mA loop

4-20mA loop

24V
COM
24V

24V→12V

TB 2-2 TB 2-3

FI (Diag. A)

TB 2-6
TB 2-3

+12V

COM

700 mA
12V

J1-1 J1-2

12V Supply

12V

COM

AO: 0-10V

AO: COM

Analog Output: Valve

A1 A2 A3 A4 A5 A6

2 4 6 24

1 3 5 23

Red - Power
Blk - Return
Wht - TX (Out)
Grn - RX (In)
Blu - Rly 1
Org - Rly 2
Yel - Rly 3
Pur - Rly 4
Brn - Rly Com

Table A: LT cable color coding

TB2
1 EXC OUT
2 SIG IN
3 SIG RTN
4 RST IN
5 EXT GATE
6 BATTERY

EXCITATION= 5.0V
LOW LEVEL SIGNAL
ZERO THRESHOLD
NO FILTER
243K PULL-UP RESISTOR TO +EXC.

1 CLOSED
2 OPEN
3 CLOSED
4 OPEN
5 OPEN
6 OPEN
7 OPEN
8 OPEN
9 OPEN
10 OPEN

S1
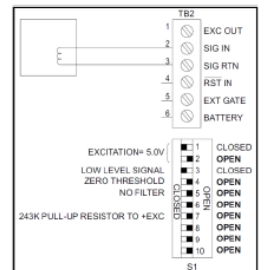
Diagram A: FI connection diagram

POWER OUTPUT 1 OUTPUT 2
L(+) N(-) NO NC C NO NC C
8 7 6 5 4 3 2 1

PROCESS (CURRENT)

1(-) 2 3 4 5 6 7(+)
INPUT

External Excitation
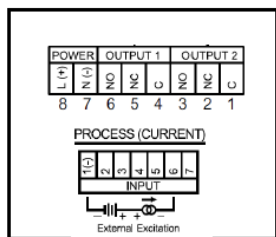
Diagram B: PI connection diagram

REVISED
3/8/2012

Design/Draft: F. Arvani January 26, 2012

Pump Station (45gpm, 1000psi) Control/Instrumentation Circuit

SIZE | FSCM NO | DWG NO | REV

SCALE 1:1 SHEET 1 OF 1

A-13.   Mobile DAQ System Operation Manual

Steps:

1. In operation, all the connections should be connected and checked. Then turn on the power switch, and the light will be on.

2. Click on the NI network browser icon.

Make sure the device is in the list and record the IP Address for future usage.

3. Click on the NI MAX icon.

On the left, My System - Devices and Interfaces - Network Devices

NI cDAQ-9188 "xxxxxxxx"

1: NI 9237 "xxxxxxxx"

8: NI 9205 (DSUB) "xxxxxxxx"

Make sure they all work. If not, delete the NI cDAQ-9188 and My System - Devices and Interfaces - Network Devices – Add Network Device – Find Network NI-DAQmx Devices. The IP address will be used if the NI module does not show up in the list.

4. After the devices are ready, click the

and wait for the program to start.

5. Click Run to run the program (Run will change to Stop), and click Record to record the data.

6. After clicking Record, the system will ask you to select a channel to be recorded, the file location and the file name, making the work clear and keeping every file for the sake of future benefit.

7. Click Record again to stop recording.

8. Click Stop to stop the program.

9. If one file is wrong it can be deleted only when the program is stopped.

10. Save all the data and shut down the system.

11. Disassemble the system and store it safely.

A-14.   Master Arduino Board Program

```
#include <SPI.h>

#include <Wire.h>


int CSArray[3] = {8,9,10};


char POWER_CTL = 0x2D;       //Power Control Register

char DATA_FORMAT = 0x31;

char DATAX0 = 0x32;     //X-Axis Data 0

char DATAX1 = 0x33;     //X-Axis Data 1

char DATAY0 = 0x34;     //Y-Axis Data 0

char DATAY1 = 0x35;     //Y-Axis Data 1

char DATAZ0 = 0x36;     //Z-Axis Data 0

char DATAZ1 = 0x37;     //Z-Axis Data 1


//This buffer will hold values read from the ADXL345 registers.

char values [15];

char buffer [8];


int SSpin = 11;     // magnetometer pin 4

int DRDYpin = 12;       // magnetometer pin 5

//int RESETpin = 13;     // magnetometer pin 6

int heading = 0;    // magnetic field heading
```

```
void setup()

{

    Wire.begin();

    //Initiate an SPI communication instance.

    SPI.begin();

    //Configure the SPI connection for the ADXL345.

    SPI.setDataMode(SPI_MODE3);

    //set the SPI connection to fast.

    SPI.setClockDivider(SPI_CLOCK_DIV2);

    //Create a serial connection to display the data on the terminal.

    Serial.begin(9600);


    pinMode(SSpin, OUTPUT);

    pinMode(DRDYpin, INPUT);



        pinMode(CSArray[0], OUTPUT);

        digitalWrite(CSArray[0], HIGH);

        writeRegister(POWER_CTL, 0x08,CSArray[0]);

        writeRegister(DATA_FORMAT, 0x01,CSArray[0]);


        pinMode(CSArray[1], OUTPUT);
```

```
digitalWrite(CSArray[1], HIGH);

writeRegister(POWER_CTL, 0x08,CSArray[1]);

writeRegister(DATA_FORMAT, 0x01,CSArray[1]);


pinMode(CSArray[2], OUTPUT);

digitalWrite(CSArray[2], HIGH);

writeRegister(POWER_CTL, 0x08,CSArray[2]);

writeRegister(DATA_FORMAT, 0x03,CSArray[2]);


digitalWrite(SSpin, LOW);

SPI.transfer(0x00);

SPI.transfer(0x9C);

digitalWrite(SSpin, HIGH);

delay(10);


digitalWrite(SSpin, LOW);

SPI.transfer(0x01);

SPI.transfer(0x20);

digitalWrite(SSpin, HIGH);

delay(10);


digitalWrite(SSpin, LOW);

SPI.transfer(0x02);
```

```
            SPI.transfer(0x00);

            digitalWrite(SSpin, HIGH);

    }



void loop()

{

//   heading = getHeading(x, y, z);    // calculates the magnetic field heading

        Wire.beginTransmission(2); // transmit to slave device

        byte mag[6];

        readMag(mag);

        int i = 0;

        for(i = 0; i < 6; i++)

            Wire.write(mag[i]);



        int j = 0;

        for(j=0;j<3;j++)

        {

            readRegister(DATAX0, 6, values,CSArray[j]);

            int i = 0;

                for(i=0;i<6;i++)

                {

                    Wire.write(values[i]);
```

```
        }


    }

    Wire.endTransmission();      // stop transmitting

}


void writeRegister(char registerAddress, char value, int CS){

    //Set Chip Select pin low to signal the beginning of an SPI packet.

    digitalWrite(CS, LOW);

    //Transfer the register address over SPI.

    SPI.transfer(registerAddress);

    //Transfer the desired register value over SPI.

    SPI.transfer(value);

    //Set the Chip Select pin high to signal the end of an SPI packet.

    digitalWrite(CS, HIGH);

}



    //This function will read a certain number of registers starting from a specified

address and store their values in a buffer.

    //Parameters:

    //   char registerAddress - The register addresse to start the read sequence from.

    //   int numBytes - The number of registers that should be read.
```

```
//   char * values - A pointer to a buffer where the results of the operation should be
stored.

void readRegister(char registerAddress, int numBytes, char * values, int CS){

//Since we're performing a read operation, the most significant bit of the register
address should be set.

char address = 0x80 | registerAddress;

//If we're doing a multi-byte read, bit 6 needs to be set as well.

if(numBytes > 1)address = address | 0x40;


//Set the Chip select pin low to start an SPI packet.

digitalWrite(CS, LOW);

//Transfer the starting register address that needs to be read.

SPI.transfer(address);

//Continue to read registers until we've read the number specified, storing the
results to the input buffer.

for (int i=0; i<numBytes; i++){

    values[i] = SPI.transfer(0x00);

}

//Set the Chips Select pin high to end the SPI packet.

digitalWrite(CS, HIGH);

}


int readMag(byte result[])
```

```
{
    digitalWrite(SSpin, LOW);

    SPI.transfer(0xC3);

    result[0] = SPI.transfer(0xFF);

    result[1] = SPI.transfer(0xFF);

    result[2] = SPI.transfer(0xFF);

    result[3] = SPI.transfer(0xFF);

    result[4] = SPI.transfer(0xFF);

    result[5] = SPI.transfer(0xFF);

    digitalWrite(SSpin, HIGH);

    return 0;
}


int receiveBit()

{
    // receive the data on the FALLING edge of the clock
char value;

    int bit = SPI.transfer(0x00);


    return bit;
}
```

A-15.   Slave Arduino Board Program

```
#include <Wire.h>

#include <SD.h>

#include <SPI.h>


const int chipSelect = 10;

//make a string for assembling the data to log:

String dataString = "";

short receiveFlag = 0;

short mx,my,mz;

short acc1x,acc1y,acc1z;

short acc2x,acc2y,acc2z;

short acc3x,acc3y,acc3z;


File dataFile;


void setup()

{

   Wire.begin(2);                        // join i2c bus with address #4

   SPI.begin();

   //Configure the SPI connection for the ADXL345.

   SPI.setDataMode(SPI_MODE3);

   //set the SPI connection to fast.
```

```
SPI.setClockDivider(SPI_CLOCK_DIV2);

//Create a serial connection to display the data on the terminal.


Wire.onReceive(receiveEvent); // register event

Serial.begin(9600);                    // start serial for output


if (!SD.begin(chipSelect)) {

  while (1) ;

}


// Open up the file we're going to log to!

dataFile = SD.open("test.txt", FILE_WRITE);

}



void loop()

{

    if (receiveFlag = 1)

    {

    dataFile.print(millis());

    dataFile.print(',');

    dataFile.print(mx);

    dataFile.print(',');
```

```
dataFile.print(my);

dataFile.print(',');

dataFile.print(mz);

dataFile.print(',');

dataFile.print(acc1x);

dataFile.print(',');

dataFile.print(acc1y);

dataFile.print(',');

dataFile.print(acc1z);

dataFile.print(',');

dataFile.print(acc2x);

dataFile.print(',');

dataFile.print(acc2y);

dataFile.print(',');

dataFile.print(acc2z);

dataFile.print(',');

dataFile.print(acc3x);

dataFile.print(',');

dataFile.print(acc3y);

dataFile.print(',');

dataFile.println(acc3z);


}
```

```
    dataFile.flush();

  }



// function that executes whenever data is received from master

// this function is registered as an event, see setup()

void receiveEvent(int howMany)

{

  while(1 <= Wire.available()) // loop through all but the last

  {

    mx = ((Wire.read() << 8) | Wire.read());

    mz = ((Wire.read() << 8) | Wire.read());

    my = ((Wire.read() << 8) | Wire.read());


    acc1x = Wire.read() | (Wire.read() << 8);

    acc1y = Wire.read() | (Wire.read() << 8);

    acc1z = Wire.read() | (Wire.read() << 8);


    acc2x = Wire.read() | (Wire.read() << 8);

    acc2y = Wire.read() | (Wire.read() << 8);

    acc2z = Wire.read() | (Wire.read() << 8);


    acc3x = Wire.read() | (Wire.read() << 8);
```

```
acc3y = Wire.read() | (Wire.read() << 8);

acc3z = Wire.read() | (Wire.read() << 8);



receiveFlag = 1;



  }

}
```

A-16. Sensor Sub Connection Diagram
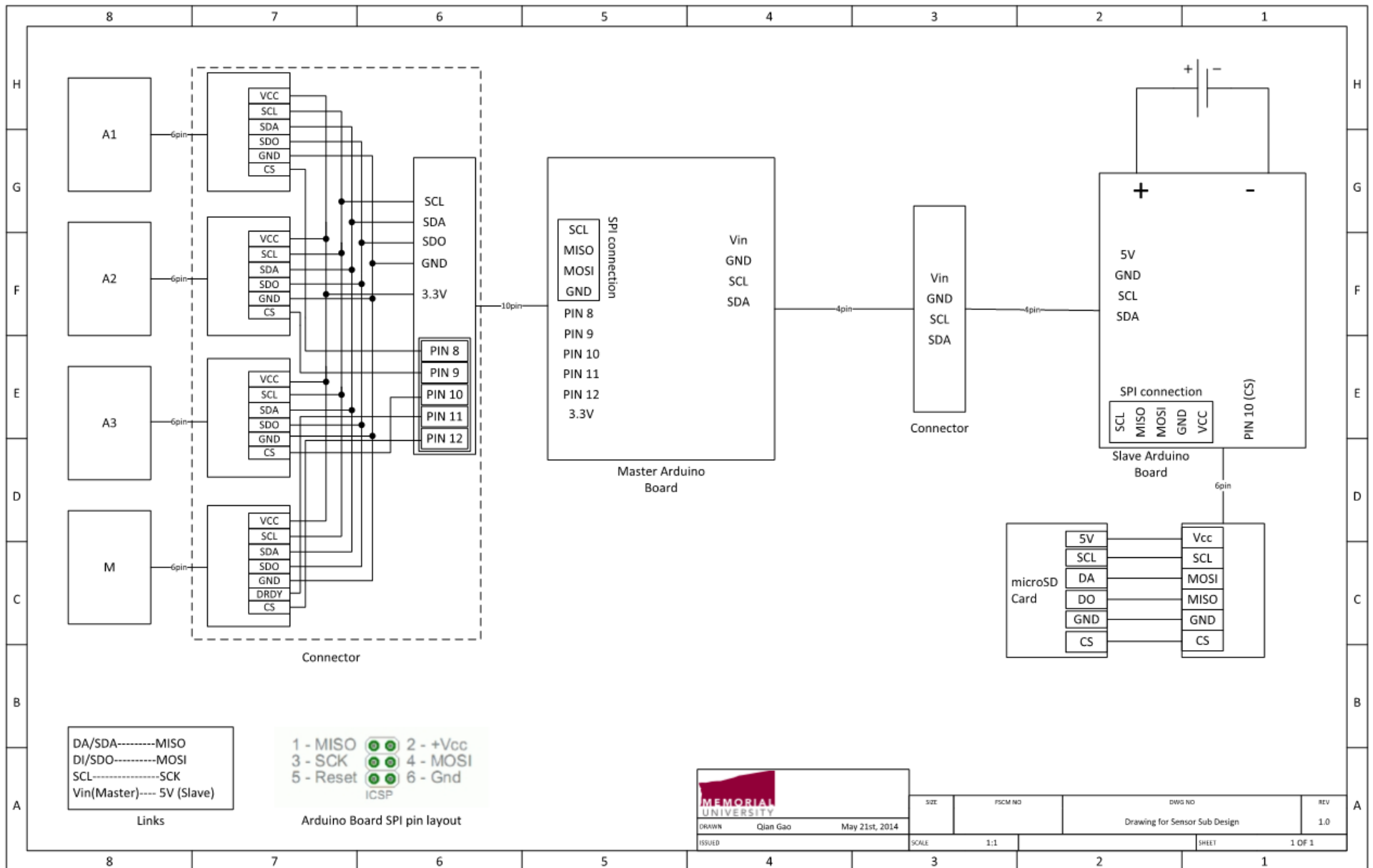
A-17. I 9205 DAQ Module Specifications Summary

General	
Product Family	Industrial I / O
Measurement Type	Voltage
Form Factor	CompactDAQ CompactRIO
Operating System / Target	Real-Time Windows
RoHS Compliant	No
Isolation Type	Ch-Earth Ground Isolation
Analog Input	
Single-Ended Channels	32
Differential Channels	16
Analog Input Resolution	16 bits
Maximum Voltage Range	
Range	-10 V - 10 V
Accuracy	6220 μV

General	
Minimum Voltage Range	
Range	-0.2 V - 0.2 V
Accuracy	157 μV
Simultaneous Sampling	No
Timing / Triggering / Synchronization	
Triggering	Analog
Physical Specifications	
Length	9 cm
Width	2.3 cm
I / O Connector	36-position spring terminal 37-pin D-Sub
Operating Temperature	-40 ℃ - 70 ℃

A-18.   NI 9237 DAQ Module Specifications Summary

General	
Product Family	Industrial I / O
Measurement Type	Strain / Bridge-based sensor
Form Factor	CompactDAQ CompactRIO
Operating System / Target	Real-Time Windows
RoHS Compliant	Yes
Isolation Type	Ch-Earth Ground Isolation
Analog Input	
Single-Ended Channels	0
Differential Channels	4
Analog Input Resolution	24 bits
Maximum Voltage Range	
Range	-25 mV / V - 25 mV / V

General	
Accuracy	0.0375 mV / V
Bridge Configurations	Full Bridge
	Half Bridge
	Quarter Bridge
Simultaneous Sampling	Yes
Excitation Voltage	2 V
	2.5 V
	3.3 V
	5 V
	10 V
Signal Conditioning	Anti-aliasing filter
	Bridge completion
	Voltage excitation
Physical Specifications	
Length	9 cm
Width	2.3 cm

General	
I / O Connector	RJ50
Operating Temperature	-40 ℃ - 70 ℃